



Using leaf margin analysis to estimate the mid-Cretaceous (Albian) paleolatitude of the Baja BC block

Ian M. Miller*, Mark T. Brandon, Leo J. Hickey

Yale University, Department of Geology and Geophysics, P.O. Box 208109, New Haven, CT 06520-8109, USA

Received 25 December 2004; received in revised form 1 February 2006; accepted 14 February 2006

Available online 19 April 2006

Editor: E. Boyle

Abstract

The “Baja BC hypothesis”, which postulates that western Washington State, British Columbia and southern Alaska originated at the latitude of Mexico, has pitted paleomagnetic results against long-held interpretations about the tectonic evolution of western North America. In this paper we develop a new paleobotanical method for estimating paleolatitude and apply it to this problem. We start by showing that the modern *MAT* field for North America is well correlated with latitude, demonstrating the feasibility of using *MAT* to estimate paleolatitude. A compilation of *MAT* and floral data from 84 modern sites in Central and North America is used to establish a new prediction relationship, $MAT = 1.32 + 28.99P$, where *P* is the proportion of smooth-margined species within a floral sample at a site. Our analysis also includes a more complete estimate of the uncertainties associated with estimating *MAT* from a measurement of *P*. Using modern data, we show that *MAT* and *P* can be used to estimate latitude as well. We then apply this approach to resolve the paleolatitude of Baja BC. Eleven floral sites from stable North America are used to establish the latitudinal *MAT* profile for North America during the Albian and Cenomanian. A floral site from the Winthrop Formation, a mid-Cretaceous (110–100 Ma) fluvial unit in the Methow basin of northern Washington State, is linked to the Baja BC block and predates its proposed northward offset. Forty-three morphospecies of dicotyledonous angiosperm leaves from the Winthrop Formation give $P = 0.76$, which is equivalent to a *MAT* of 23.4 °C, indicating a subtropical to tropical climate. We use the North American *MAT* profile to estimate a paleolatitude of 38.4°N for the Winthrop flora, indicating ~2200 km of northward offset relative to stable North America.

© 2006 Elsevier B.V. All rights reserved.

Keywords: mean annual temperature; leaf margin analysis; Baja BC block; Winthrop Formation; Methow basin; Albian stage; Washington state; paleobotany

1. Introduction

The geology of southern Alaska, western British Columbia, and western Washington State was assembled during a major accretionary event at 100 to 85 Ma. This event is marked by the collision of the Insular superterrane (orange unit in Fig. 1) and other smaller

terrane with the west coast of North America (NA), and the formation of the Coast Mountains orogen (yellow unit), which extends from western Washington to southern Alaska [1]. Geologists have long recognized that, after this Late Cretaceous accretion, the more outboard parts of the Northwest Cordillera were displaced northward along the North American margin. Motion on recognized strike-slip faults (e.g., Pinchi fault, Rocky Mountain Trench, Tintina fault, Straight Creek–Fraser fault, Fig. 1) account for an estimated

* Corresponding author. Fax: +1 203 432 3134.

E-mail address: ian.miller@yale.edu (I.M. Miller).

~ 500 to 1000 km of post-collisional northward motion [2,3].

A major problem with this interpretation is that paleomagnetic data accumulated over the last 30 yrs indicate much larger offsets after 85 Ma, involving ~ 2500 km of northward transport [4–13]. Some argue that geologic evidence does not allow for such large, young offsets [3,14] but as of yet there are no definitive geologic ties that preclude the proposed ~ 2500 km offset of the Insular superterrane and the Coast Mountain orogen [1,15]. Others contend that the discrepancy is due to problems with paleomagnetic measurements, such as unresolved tilting of plutons and inclination flattening in sedimentary units [16–18]. These issues have been largely addressed [5,6,12] and the corrected paleomagnetic data still show large northward transport. These results are also in agreement

with those from a volcanic unit [7] in Baja BC, where paleohorizontal is known and inclination flattening is unlikely. Impressively, even after close scrutiny, four independent areas within the Baja BC block (MS, MT, DI, NG in Fig. 1) all indicate ~ 2500 km of northward offset after ~ 90 Ma. A detailed study of the MacColl Ridge Formation in southern Alaska [19] (MC in Fig. 1) also suggests a significant but smaller offset. However, the magnetization age of this site is relatively young (~ 79 Ma) and thus may not record the full offset [20].

The Baja BC debate remains one of the most contentious issues about the tectonic evolution of western NA. The reconstructions in Fig. 1 help illustrate what is at stake. Abbreviations indicate the main paleomagnetic studies for this time period, as summarized in Table 1. Fig. 1A shows the modern disposition of major pre-Cenozoic terranes of western NA and the

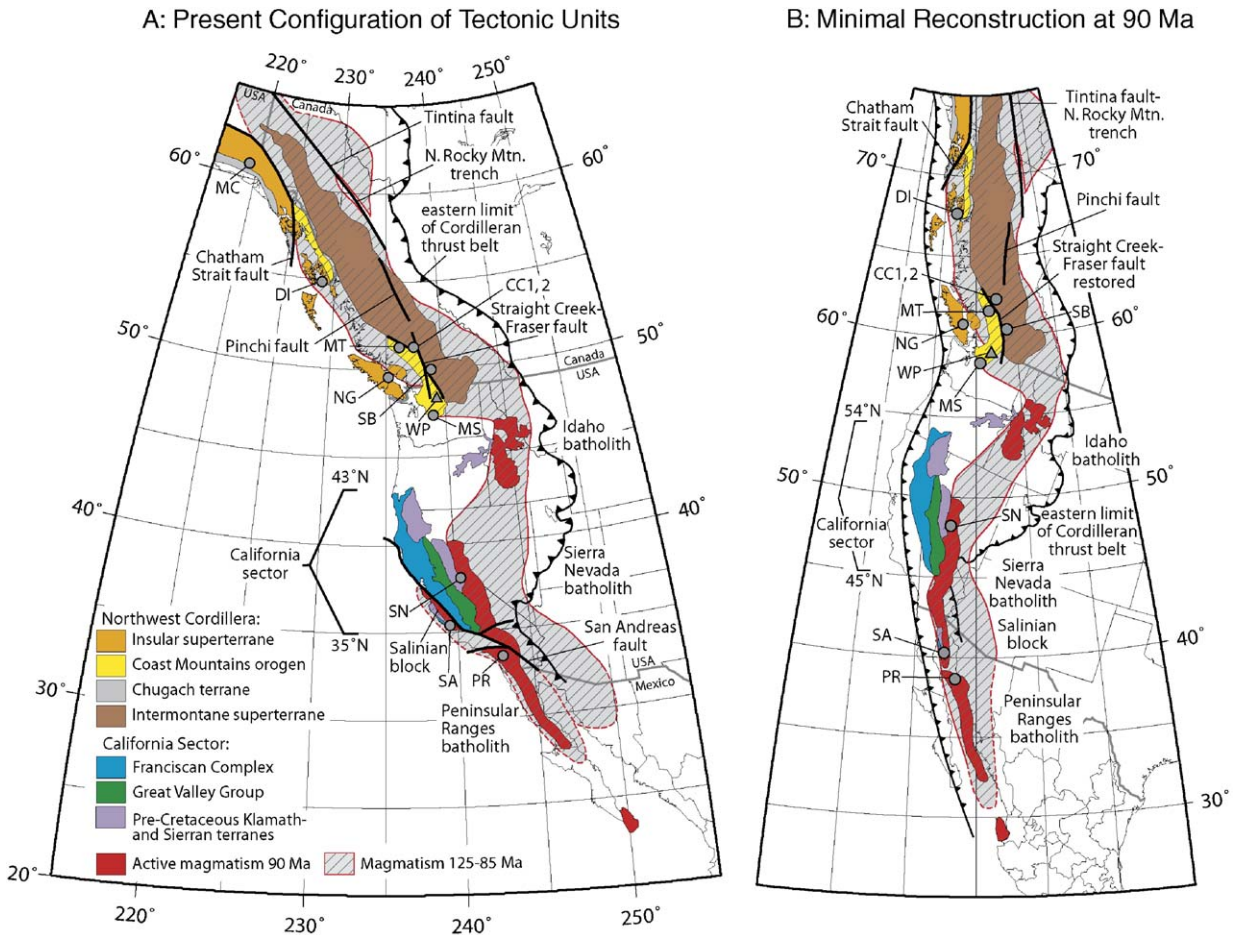


Fig. 1. Tectonic maps showing present disposition and reconstructions of tectonic units in western NA. The following sources were used to construct these maps: tectonic units [1,84,85], the eastern Cordilleran thrust front and the locus of magmatism at 125–85 Ma [86], the 125–85 Ma pole position for NA [6], and Cenozoic Basin and Range extension [87]. The maps were created using GMT [88]. Gray circles show the location of paleomagnetic sites relevant to our 90 Ma reconstructions. Abbreviations and data are summarized in Table 1. The gray triangle shows the location of the Winthrop flora (WP).

C: Full Reconstruction, Northern Option at 90 Ma

D: Full Reconstruction, Southern Option at 90 Ma

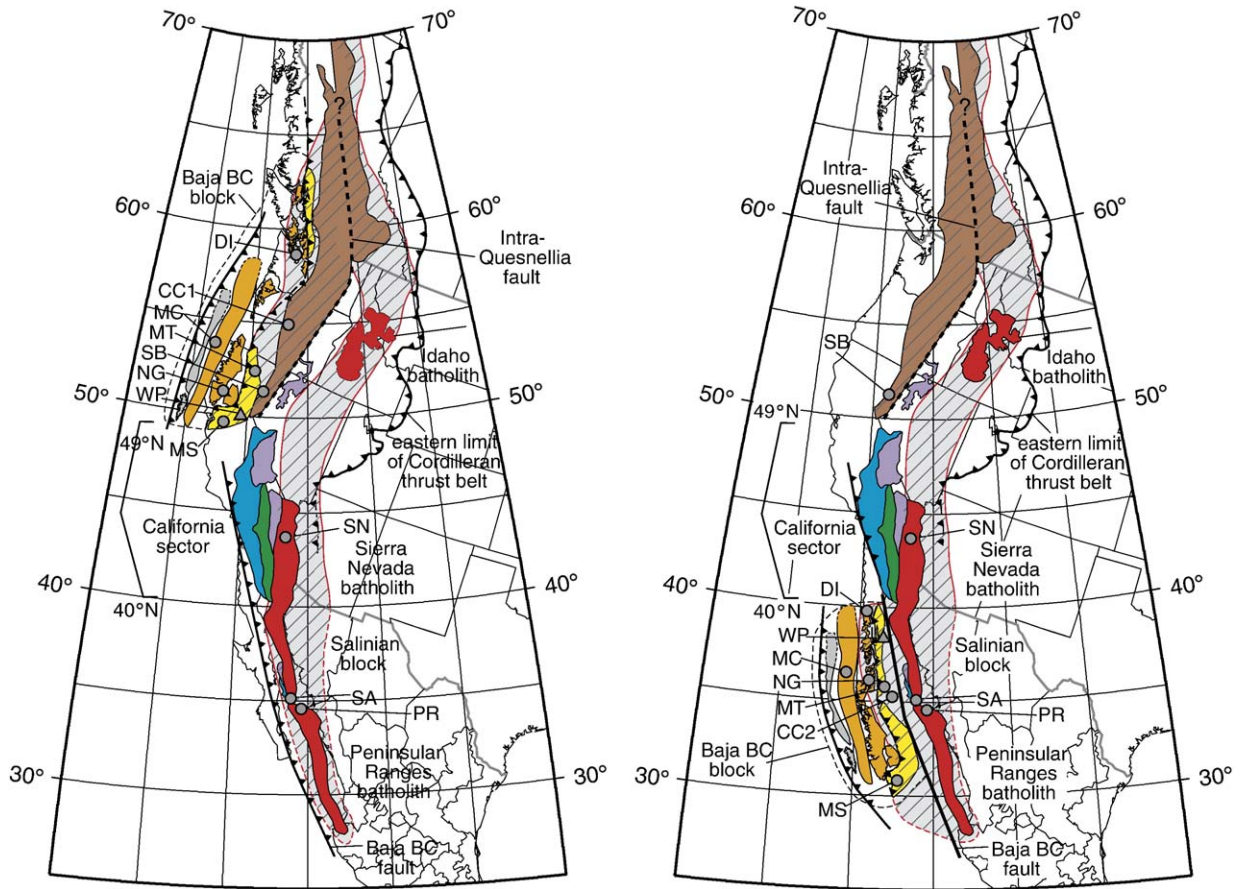


Fig. 1 (continued).

contemporaneous mid-Cretaceous magmatic arc. Fig. 1B–D show various reconstructions for 90 Ma. Stable NA has been restored using the mid-Cretaceous pole from Housen et al. [6]. Fig. 1B shows that at 90 Ma, if the Baja block moved with stable NA it would be about 10° north of its present latitude. In Table 1, we report only the paleomagnetically determined paleolatitudes rather than the estimated offsets relative to stable NA because there is nothing within the western Cordillera that was fixed with respect to stable NA. Fig. 1B shows a minimal reconstruction, accounting for the motion of the NA plate and removal of Cenozoic Basin-and-Range extension, motion on the San Andreas and associated faults, and ~100 km of right-lateral slip on the Straight Creek–Fraser fault. This map provides a reference point from which to judge the more comprehensive reconstructions that follow.

Fig. 1C and D show the main competing reconstructions for western NA at 90 Ma [1]—the Northern and Southern Options. We differ from [1] in that we

place the 90 Ma magmatic arc at the paleolatitudes indicated by the paleomagnetic sites SN, SA and PR (Table 1). Both include restoration of ~1000 km of motion on a set of faults within the Intermontane superterrane, which Irving et al. [21] loosely called the “Intra-Quesnellia fault” (see also [1]). This fault might be better viewed as a broad shear zone that involved motion on main orogen-parallel faults, such as the Pinichi, Rocky Mountain Trench, and Tintina faults. The western offset part of the Intermontane superterrane is conveniently termed the Alta BC block in [1,22]. Paleomagnetic data from the Spences Bridge volcanics [21] (SB in Figure) are consistent with this restoration of Alta BC.

The Baja BC block lies farther to the west. As noted earlier, all of the terranes within the Baja BC block were assembled by ~90 Ma, so it can be easily identified and tracked as a single block when analyzing offsets after that time [1]. The boundary between Baja BC and Alta BC is difficult to resolve,

Table 1
Paleomagnetic results used for 90 Ma reconstruction of western North America

Paleomagnetic study, location, and references	Magnetization age (Ma)	Measured paleolatitude (°N, 95% CI)
<i>Baja BC block, Washington State and southern British Columbia</i>		
MS: Mount Stuart batholith, Washington State, Housen et al. [6]	91	31.3(−3.4/+3.8)
MT: Mount Tatlow, SW British Columbia, Wynne et al. [7]	100–84	(35.9±3.5)
DI: Duke Island ultramafic complex, Alaska, Bogue and Grommé [9]	110	(43.9±16.0)
NG: Nanaimo Supergroup, Vancouver Island, Krijgsman and Tauxe [12]	84–72	36.0(−7.0/+9.0)
CC2: Conglomerates of Churn Creek, SW British Columbia, Enkin et al. [13]	95–85	(36.1±2.4)
<i>Baja BC block, offset to southern Alaska (“Baja Alaska”)</i>		
MC: MacColl Ridge Formation, SE Alaska, Stamatakos et al. [19]	79	(53±8)
<i>Alta BC block of western Canada</i>		
CC1: Volcanics of Churn Creek, SW British Columbia, Haskin et al. [25]	105–100	(55.0±3.9)
SB: Spences Bridge volcanics, S British Columbia, Irving et al. [21]	104	(50.8±5.0)
<i>Mid-Cretaceous magmatic arc batholiths in California and northwestern Mexico</i>		
SN: Sierra Nevada batholith, California, Frei et al. [78], Frei [79]	100–90	(42.9±5.0)
SA: Salinian block, California, Whidden et al. [80]	83	(34.9±4.8)
PR: Peninsular Ranges batholith, California, Teissere and Beck [81], Hagstrum et al. [82], Ague and Brandon [83]	120–100	(34.8±3.3)

because of young magmatism in the Coast Mountains and North Cascades, Eocene extension in the southern British Columbia and Washington State, and generally poor exposure [1,14,15].

Paleomagnetic data for the Baja BC block (Table 1) are largely consistent with the restoration shown in the Southern Option (Fig. 1D), where the Baja BC block is located south of the California sector, as marked by the Sierra Nevada batholith, the Great Valley forearc basin, and the Franciscan subduction complex. Cowan et al. [1] argued that the Baja BC block must have originated either north or south of the “California sector,” given the record of active subduction from ~150 to 90 Ma. Umhoefer [22] has suggested that subduction was inactive along the California sector at 100 to 90 Ma, thus permitting Baja BC to be located west of California at that time. As reviewed in [1], the evidence for continuous active subduction from 150 to 90 Ma remains compelling.

Another recent interpretation is that at ~105 Ma the Baja BC block was contiguous with the Alta BC block to the east, as shown in the Northern Option (Fig. 1C). Then, between 105 and 90 Ma, the Baja BC block was transported southward ~1500 km before returning to its original location opposite Alta BC by 50 Ma. This interpretation is consistent with a far-traveled Baja BC, but postulates a more complex displacement history.

This “yo-yo” interpretation is based on two paleomagnetic studies in the Churn Creek area in SW British Columbia (CC1 and CC2 in Fig. 1). The volcanic rocks of Churn Creek (105 to 100 Ma) appear to be equivalent to

the coeval Spences Bridge volcanics in Alta BC (CC1 and SB, respectively, in Fig. 1). Paleomagnetic data indicate that these units originated at similar paleolatitudes (Table 1). Younger conglomerates (95 to 85 Ma) that overlie the volcanics of Churn Creek give a much lower paleolatitude (CC2 in Table 1), which matches the paleolatitude determined from the Mount Tatlow section (MT in Table 1 and Fig. 1), located in the Baja BC block just to the west of Churn Creek. Mahoney et al. [23] have argued that the Silverquick conglomerate in the Mount Tatlow section is equivalent to the conglomerates at Churn Creek. This correlation is difficult to judge because similar conglomerates are found throughout southern British Columbia and NW Washington State. Furthermore, the two units are separated by the Yalakom fault, which is a major but otherwise poorly known strike-slip fault. We acknowledge, however, that the similarity in the paleomagnetically determined paleolatitudes for the Silverquick conglomerate and the conglomerates of Churn Creek (MT and CC2 in Table 1) provide additional support for the correlation of these units.

The “yo-yo” interpretation for the Baja BC block rests mainly on the conclusion that the volcanics and conglomerates at Churn Creek are part of a single stratigraphic section. Riesterer et al. [24] document this relationship at one location (see Fig. 5, section in [24]), where about 30 m of conglomerate can be observed in direct depositional contact with the underlying volcanics of Churn Creek. However, this is the only depositional contact that has been found between the units. The paleomagnetic sites of Enkin et al. [13] were located in

exposures of the conglomerate that cannot be tied directly to the volcanics of Churn Creek. This point is important because we conclude below that during the Albian, the Winthrop Formation was being deposited at low latitudes ($\sim 38^\circ\text{N}$) while the volcanics of Churn Creek were being erupted at moderate latitudes ($\sim 55^\circ\text{N}$). Haskin et al. [25] and Enkin et al. [13] make compelling arguments that all of these units (WP, CC1, CC2 in Fig. 1) were deposited in the Methow–Tyaughton basin, which was an elongate synorogenic basin that flanked the east side of the Coast Mountains orogen. The results from these sites highlight a significant paleolatitudinal discrepancy in pre-90 Ma Baja BC reconstructions.

Biogeography and provenance studies are available to assess various reconstructions of the western NA Cordillera. Rudistid mollusks [18], radiolarians (see Ref. [26]), and palynomorphs [27] have been used to estimate the paleolatitude of Cordilleran terranes, but results are generally of low resolution or are only loosely related to the transport history of the Baja BC block. Two papers [28,29] have attempted to use U/Pb dating of detrital zircons to directly estimate the location of Baja BC during the Cretaceous. Mahoney et al. [28] argued for a northern position for Baja BC based on detrital U/Pb zircon ages for the Nanaimo Supergroup (NG in Fig. 1) but Housen and Beck [29] showed that the Mahoney et al. [28] results were also consistent with northward transport of Baja BC from an originally low latitude position. More recently, DeGraaf-Surpless et al. [30] argued that detrital U/Pb zircon ages in the Methow basin indicated that it was fed by sediments derived from eastern sources in southern Canada. This result is odd given that even the most conservative interpretations would place the Methow–Tyaughton basin some 1000 km south of these proposed southern Canadian sources (e.g., Fig. 1C). In the Northern Option (Fig. 1C), the Idaho batholith would lie directly to the east, but the detrital U/Pb zircon ages in the Methow basin reported by DeGraaf-Surpless et al. [30] do not match those expected from an Idaho batholith source (see Fig. 10 in [30]). Assessment of the Southern Option for Baja BC (Fig. 1D) using detrital U/Pb zircon ages would require information about the basement geology of NW Mexico. This area is widely covered by Eocene and younger volcanic rocks [31] making it difficult to fully assess older U/Pb zircon source terrains that would have been exposed during the mid-Cretaceous when the Methow samples studied in [30] were being deposited.

In this study, we use paleobotanical estimates of mean annual temperature (*MAT*) from angiosperm leaf fossils from the Winthrop Formation, in the Methow

basin (Figs. 1 and 2A, B), to estimate the paleolatitude of the Baja BC block. This approach relies on two relationships. First, *MAT* is mainly a function of latitude and elevation [32,33]. In other words, at similar elevation, meridional variations are large, and zonal variations are small. Other studies (B.T. Otto-Bliesner, pers. commun., 2003, [35]) indicate that the meridional temperature gradient during the middle Cretaceous was $\sim 0.45^\circ\text{C}/^\circ\text{N}$. Thus, the 1500 km difference between the Northern and Southern Options for the Baja BC block (Fig. 1) is equivalent to a difference in *MAT* of 6 °C. Second, *MAT* can be reliably estimated using leaf-margin analysis of fossil leaves (e.g., [36–38]). Past work indicates that the correlation between leaf margins and *MAT* is (1) insensitive to short-term (<0.5 ka) temperature anomalies, (2) unaffected by diagenetic alteration, and (3) based on a physiological mechanism that has been evolutionarily conserved since at least 100 Ma [36,39]. Our approach is further supported by the close correspondence between leaf-margin estimates of *MAT* in continental settings and coeval marine paleotemperature measurements determined from oxygen isotopes (e.g., [40]).

There are three parts to this paper. First, we use modern floral data to calibrate the relationship between leaf-margin measurements, *MAT* and latitude. The main objective is to establish a more complete estimate of the uncertainties associated with using paleofloral data to predict *MAT* and latitude. Next, we use fossil floras to estimate meridional profiles for *MAT* and *P* for stable NA in the Albian and Cenomanian. Finally, we use new leaf-margin measurements from the Winthrop flora, together with our NA meridional thermal profile, to estimate the paleolatitude of the Baja BC block at ~ 105 Ma.

2. Leaf-margin analysis: methodology and modification

In the early twentieth century, Bailey and Sinnott [41] recognized that the architecture of dicotyledonous angiosperm leaves was strongly correlated with climate. Wolfe [38] provided the first comprehensive quantitative study of this relationship using modern floral samples from many east Asian localities. He used the proportion *P* to characterize the distribution of leaf margin types by species in a sample collected by location. *P* is defined as

$$P = \frac{r}{n}, \quad (1)$$

where *n* is the total number of dicot species in the sample, *r* is the number of those species with smooth-

margined leaves and $(n-r)$ is the number of species with serrated or toothed-margined leaves. Sometimes a single species will have both smooth and serrated leaves. These mixed character species are represented in r by a score of 0.5, rather than 1.

Wolfe [38] found that P was most strongly correlated with MAT ($R^2=0.98$ as reported by Wing and Greenwood [37]) and proposed that this relationship was the result of a physiological adaptation to local climate, as represented by MAT . Wolfe [36,42] introduced an expanded method called the Climate Leaf Analysis Multivariate Program (CLAMP), which uses 31 leaf physiognomic characters from a sample of leaves to predict climatic parameters, including MAT . Wolfe [42] found using an eigenvector analysis that MAT and P are the two most strongly correlated variables in the CLAMP dataset. Wilf [43] showed that MAT can be precisely estimated using P alone. Thus, the strong correlation between P and MAT observed in modern leaf studies provides a confident basis for estimating paleo- MAT using fossil leaves (e.g., [40,45,46]).

Wilf [43] reported a more detailed analysis of the relationship of P with MAT . His study included nine sites with n ranging from 74 to 629. In comparison, Wolfe's studies typically had n ranging from 20 to 40. These different studies provide an ideal basis to look at the errors and uncertainties associated with estimating P and MAT . Fig. 2A shows a compilation of P and MAT values ($N=84$, where N indicates number of samples) for modern settings in North and Central America. These data are from [36,43] and are compiled in Tables A1 and A2 (see Appendix A in data repository). Note that we have excluded samples where n was not reported.

The plot shows an excellent correlation between P and MAT supporting the inference of a linear relationship between these variables,

$$P_i = a_0 + a_1 MAT_i + \varepsilon_i, \quad (2)$$

where a_0 and a_1 are unknown parameters and ε_i is the random error or misfit in the i th floral sample, where i runs from 1 to N . Our objective is to calibrate this relationship by applying the least-squares method to the modern floral data to find best-fit values for a_0 and a_1 . P_i is designed as the dependent variable for the least-squares fit, which means that the misfit ε_i is entirely attributed to errors in P_i . Previous studies (e.g., [37,38]) have regressed this relationship with MAT on the left, which implies that all of the misfit is due to error in MAT . This type of calibration will work just fine, but it does not allow a full evaluation of the errors (see Appendix A for more on this topic). Our arrangement

for (2) is based on the fact that $SE[P] \gg (dP/dMAT) SE[MAT]$, where $SE[P]$ and $SE[MAT]$ are the standard errors (or uncertainties) for a pair of P and MAT measurements. Below we show that $SE[P]$ for the data in Fig. 2 is always >0.032 and $SE[MAT]$ for NA temperature data is ~ 0.12 °C. Various least-squares fits indicate that the trend in Fig. 2A has a slope $dP/dMAT \approx 0.035$ C⁻¹. From this, we conclude that $SE[P]$ is much greater than $(dP/dMAT) SE[MAT]$ (compare >0.032 with 0.0042). We conclude that it is safe to assume that the misfit in the least-squares analysis is mainly the result of the larger errors associated with measuring P .

For calibration by least squares, it is important to account for the uncertainties associated with the different P measurements in the modern calibration dataset. The standard error $SE[P_i]$ must include, at minimum, the natural variation or "sampling error" associated with estimating P_i from a sample of limited size. If this were the only source of error, then P_i would follow a binomial distribution, so long as each leaf species in the sample was drawn from independent but otherwise identically distributed (IID) populations. In this case, $SE[P_i]$ would be defined by the binomial variance function,

$$SE[P_i]^2 = \frac{P_i(1-P_i)}{n_i}. \quad (3)$$

This uncertainty estimate was introduced for leaf-margin analysis by Wilf [43], but he emphasized that it only represented part of the total uncertainty. A common issue with binomial parameters, such as P_i , is overdispersion [47,48], which means that the variation in P_i is greater than that predicted by (3). We have investigated several models for overdispersed binary data and found that overdispersion in P_i is best represented by the logistic normal distribution [48,49], which accounts for both fixed (binomial variation) and random (extrabinomial variation) effects. $SE[P_i]$ is defined by the logistic normal variance function, which can be approximated by

$$SE[P_i]^2 = [1 + \varphi(n_i-1)P_i(1-P_i)] \frac{P_i(1-P_i)}{n_i}, \quad (4)$$

when $\varphi \ll 1$ (see Refs. [48,49] for details). Overdispersion is accounted for by the factor in square brackets. The degree of overdispersion is represented by the overdispersion factor φ [38], which is assumed to have a constant value for all of the P measurements. When $\varphi=0$, (4) reduces back to the standard binomial variance function (3).

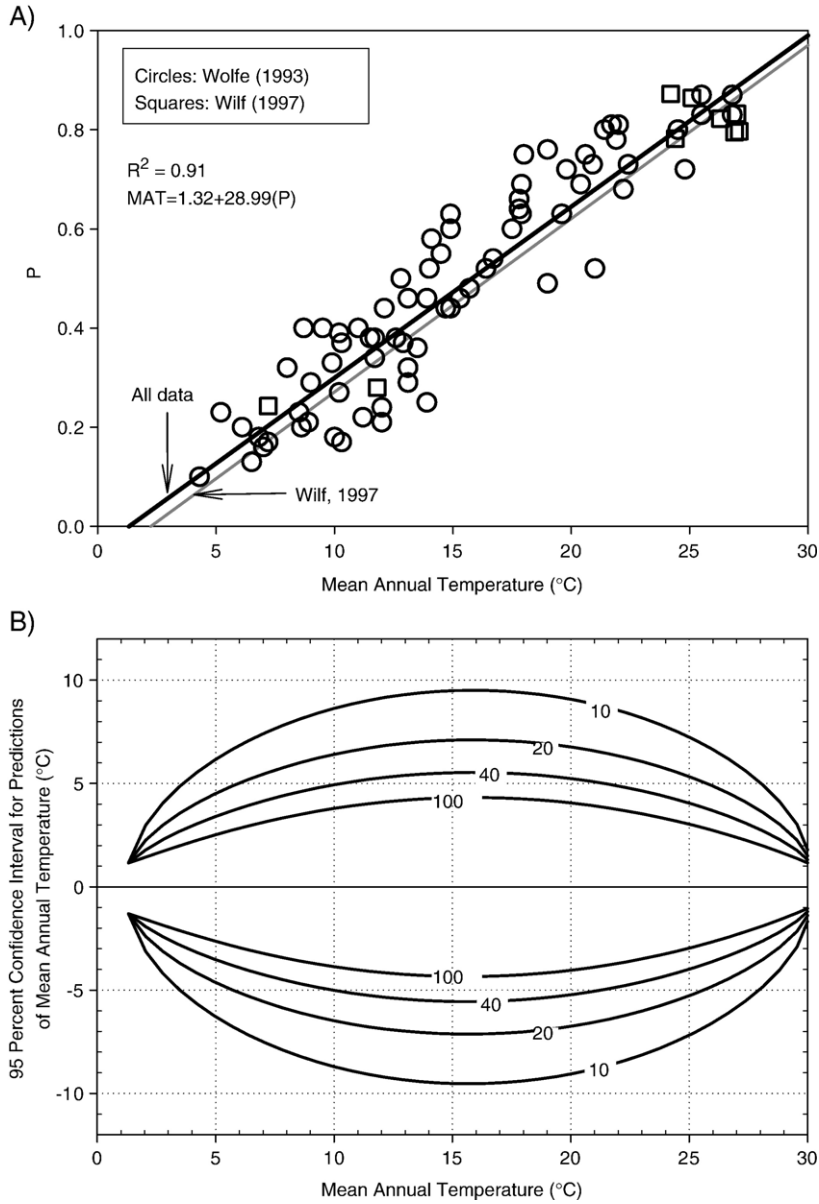


Fig. 2. (A) Modern MAT and P from floral sites in Central and North America. Open circles are CLAMP sites [36,89] and squares are from [43]. Data are tabulated in Tables A1 and A2 in Appendix A. The black line shows the best-fit for our calibration, the grey line shows the nine sites from [43] (squares). (B) Estimated uncertainties, at the 95% confidence level, for predictions of MAT using the best-fit equation above. The numbers for the contours refer to n, the number of species in the unknown sample used for the prediction.

This new specification for $SE[P_i]$ will influence the estimation of MAT from P. The quality of the least-squares fit is measured by the statistic

$$\chi_r^2 = (N-2)^{-1} \sum_{i=1}^N \left(\frac{\varepsilon_i}{SE[P_i]} \right)^2 \quad (5)$$

χ_r^2 should follow a χ^2 distribution. If the misfit errors ε_i are solely related to measurement errors in P_i , as

represented by $SE[P_i]$ from Eq. (4), then the expected value for χ_r^2 is 1.

This expectation for χ_r^2 provides the basis for estimating ϕ . First, we find a weighted least-squares solution for a_0 and a_1 with $SE[P_i]$ determined using the standard binomial variance function (3) (the weighted least-squares algorithm is described in Appendix A). This calculation gives $\chi_r^2 = 1.76$, meaning that the variance of the residuals is about 76% greater than

predicted by (3). The χ^2 distribution indicates that this value for X_r^2 has a probability of $P(\chi^2)=0.002\%$, which means that there is insignificant probability that this result could occur by random chance alone. The inference is that P_i measurements are overdispersed.

Next, we conduct an iterative search for a weighted least-squares solution for a_0 , a_1 , and φ that gives $X_r^2=1$ [48]. The results are $a_0=-0.0456\pm 0.0226$, $a_1=0.0345\pm 0.0012$ (1 SE), and $\varphi=0.052$. The fit is very good (black line in Fig. 2A), with $R^2=0.91$. The increase in the $SE[P_i]$ that comes from corrections for overdispersion is, on average, about 10% to 20% (CLAMP samples), but P_i values with $n_i>50$ (samples from [43]) show increases that range up to 160% (Fig. A1 in data repository). The parameter estimates for the calibration relationship (2) are also affected by accounting for overdispersion, given that samples with large n will have less influence in the weighted least-squares solution.

Overdispersion in binary variables is typically attributed to clustering in the sampled observations [49,50] (i.e., lack of independence or heterogeneity of data). For example, a forest will likely contain different clusters of trees of different ages (i.e., height and density of trees, sun availability), located in different microclimates, and growing under variable edaphic conditions. Thus, we would expect variations in the mean P from leaves in these different clusters, since each cluster provides a different temporal or spatial sample of the local conditions. The overdispersion effect is clear in the Wilf [43] data because the large number of sampled species permits the random effects to show up relative to the fixed effects (see Fig. A1A and B in data repository). As noted above, we tested several overdispersion models and found that the logistic normal model was the only one able to stabilize the variance of the residuals as a function of P_i and n_i .

Our objective is to use P' to predict an unknown MAT' . The calibration Eq. (2) is recast to give a prediction

$$MAT' = \frac{P' - a_0}{a_1}, \quad (6a)$$

or, using the parameters estimated above,

$$MAT' = 1.32 + 28.99P'. \quad (6b)$$

Appendix A provides an algorithm to calculate the confidence interval for an estimate of MAT' . We have used that calculation to construct Fig. 2B, which shows the 95% confidence interval (CI) for estimates of MAT' .

The plot includes uncertainties related to estimating the calibration Eq. (6b) and measuring P' , as given by $SE[P']$ using (4). The contour lines show that the 95% CI becomes progressively smaller as n gets larger. A typical study, with $n\approx 40$, will have an uncertainty of $\pm 6^\circ\text{C}$ when MAT is about 15°C , and that uncertainty will decrease to $\pm 2^\circ\text{C}$ if MAT had a more extreme value, such as 2° or 30°C .

Our analysis here provides a full inventory of the influence of random errors on the measurements of P and estimates of MAT using modern floras. This analysis should hold for paleofloral data as long as those flora are distributed in the same way as the modern flora used in the calibration dataset. We acknowledge that estimates of MAT from paleofloral samples may be subject to systematic errors [43,51], due, in large part, to different local forest environments. For example, Burnham et al. [51] has found that in the modern tropics of Ecuador, local environments adjacent to lakes and rivers have leaf distributions that would result in an underestimate of MAT by 3.5° to 5°C . Further study is needed before we can fully assess how this kind of bias might affect use of paleofloral data for estimates of MAT . A simple test used here is to see if the misfit of the variance of P in our meridional MAT reference profile for the mid-Cretaceous of NA is similar to that observed in the modern calibration dataset. Differences in variance would indicate that the paleofloral and modern floral datasets do not have the same distribution.

3. Modern mean annual temperature and latitude

Modern MAT measurements for NA were taken from a global compilation of station data [52], which contains 1944 stations from North and Central America (Fig. A2 in data repository). MAT was calculated from mean monthly temperatures for all years where all months were available. The time interval was restricted to 1900 to 2002 AD. Station data had an average record length during this time period of 69 yrs, with a range of 3 to 102 yrs. The standard deviation for MAT for each station averages 0.85°C , with a range of 0.3°C to 1.8°C . The average uncertainty for the MAT values from this dataset is $SE[MAT]\sim 0.12^\circ\text{C}$.

The contour map in Fig. 3A shows the spatial variation of MAT . Western NA shows considerable short-wavelength variability, much of which is due to topography. Modern MAT is mainly a function of latitude and elevation. Least-squares analysis was used

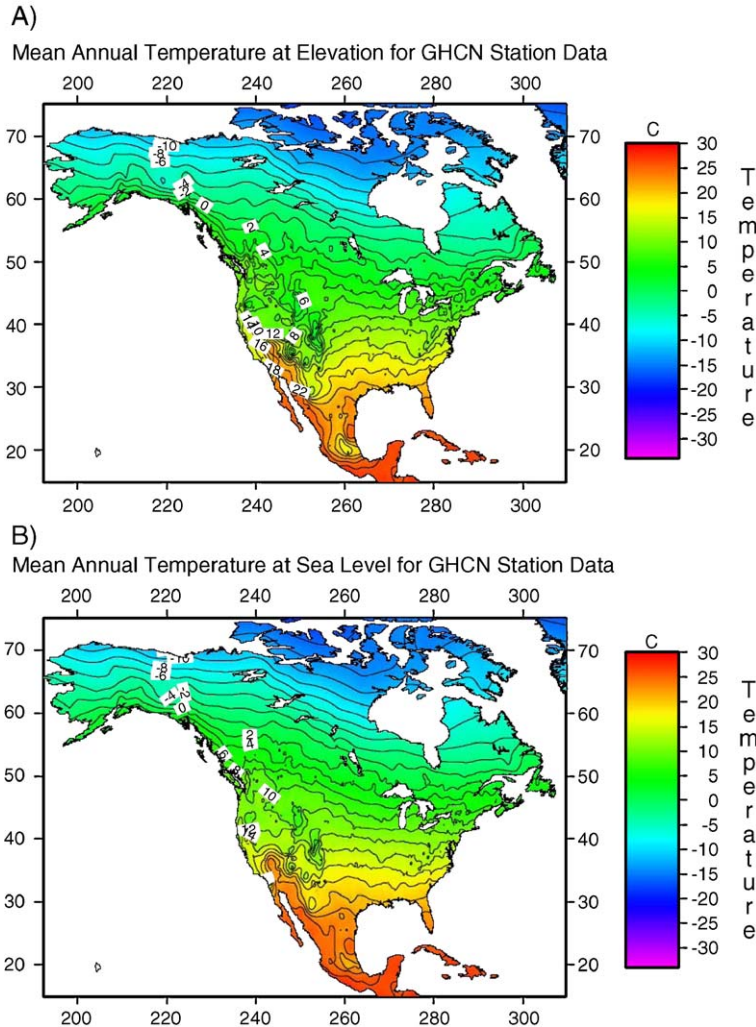


Fig. 3. Modern *MAT* from 1944 stations in NA from the Global Historical Climatology Network temperature archive version 2 dataset (v2.mean_adj.Z) [52]. (A) Contour map of *MAT* at the land surface. (B) Contour map of *MAT* corrected to sea level using a best-fit terrestrial lapse (see text for details).

to isolate the influence of these two variables. The *MAT* data are well fit ($R^2=0.89$) by a linear relationship

$$MAT = b_0 + b_1\lambda + b_2z, \quad (7)$$

where λ is latitude in degrees, and z is elevation above sea level in kilometers. The best-fit estimates and standard errors for the parameters are $b_0=41.51 \pm 0.025$ °C, $b_1=-0.734 \pm 0.0056$ °C/°latitude, and $b_2=-2.21 \pm 0.11$ °C/km. The value 2.21 °C/km represents the *MAT* lapse rate, which is the average vertical temperature gradient for the full dataset. In comparison, the global average for the free-air lapse rate in the troposphere is 6.5 °C/km, which is the expected value for the adiabatic gradient in a convecting moist atmosphere [e.g., p. 3 in Ref. 32]). Modern leaf

physiognomy (shape) datasets, particularly those including high-elevation sites, commonly use a long-term terrestrial lapse rate, as measured on the ground and averaged over many years. Our experience with the GHCN dataset is that the *MAT* lapse rate for NA varies with location from ~ 2 °C to 4.5 °C/km. The mid-Cretaceous paleofloral localities we consider below all come from locations near paleo-sea level (as indicated by the distribution of coeval marine and terrestrial sediments), so we do not need to account for this lapse rate effect. Nonetheless, we used the estimated average *MAT* lapse rate to correct the modern *MAT* data to sea level to highlight the influence of latitude on *MAT*.

The contour map of elevation-corrected *MAT* (Fig. 3B) is much smoother (Fig. 3A). Some short-

wavelength anomalies are still present (e.g., Death Valley, central Rocky Mountains), but the *MAT* distribution is now largely a function of latitude. A plot of elevation-corrected *MAT* versus latitude (Fig. 4) shows a linear trend within the northern temperate zone (23.5° to 66.5°N latitude), indicating an average meridional gradient of 0.73°C/°N (as estimated above for b_1). The trend begins to flatten near 25°N because of tropical Hadley cell circulation (p. 6 in Ref. [32]), which creates a fairly constant *MAT* (~27 °C) across the tropics (“tropical thermostat” [53–55]). Paleo-sea surface temperature measurements indicate that the tropics have maintained a constant temperature of ~27 °C back to at least 100 Ma [56]. Some recent studies do suggest significantly higher temperatures in the tropics during the mid-Cretaceous, particularly in the Cenomanian [e.g., 57]. If the long-term tropical *MAT* has remained constant, then it follows that global cooling and warming are mainly associated with changes in the meridional gradient (slope of the trend line in Fig. 4)—the poles get warmer or colder, but the tropics remain at a constant temperature.

The standard deviation of the residuals for the fit is $\sigma_r = 2.29$ °C, which is much larger than the uncertainty in the measurements (SE cited above is ~0.12 °C). The additional variation results from a pronounced zonal variation across NA at high latitudes. This is illustrated in Fig. 3B by the southward deflection of the west-to-east trend of the temperature contours at latitudes above

~40°N (Fig. 3B), and in Fig. 4 by an increase in the residuals with increasing latitude. Forest et al. [33] report a similar pattern of zonal variation in both *MAT* and humidity over modern NA. This zonal variation could be problematic for using leaf margin *MAT* data to estimate paleolatitude.

There are at least two factors that contribute to this zonal variability. Atmospheric flow above NA is dominated by the Westerlies, which describe the strong west-to-east zonal circulation in the northern temperate zone. The meridional thermal gradient is established and maintained over the Pacific Ocean because of the high-heat capacity of water and the stability of the poleward heat transport in the oceans. The Westerlies start to lose heat as they flow over the continent (i.e., the continentality effect) because of the low heat capacity of land relative to water and the absence of poleward heat transport in the continents. Zonal circulation is also affected by the north-south trending mountain ranges of NA. Seager et al. [58] showed, using an atmospheric general circulation model, that flow of the Westerlies over the Rocky Mountains causes atmospheric circulation to swing to the southeast, bringing colder temperatures to northeast NA.

Zonal variation tends to degrade our ability to use meridional profiles of *MAT* or *P* to estimate paleolatitude. This problem is partially accounted for by an increase in the estimated uncertainties for unknown paleolatitudes. In other words, zonal variation creates larger residuals in the least-squares solution and larger

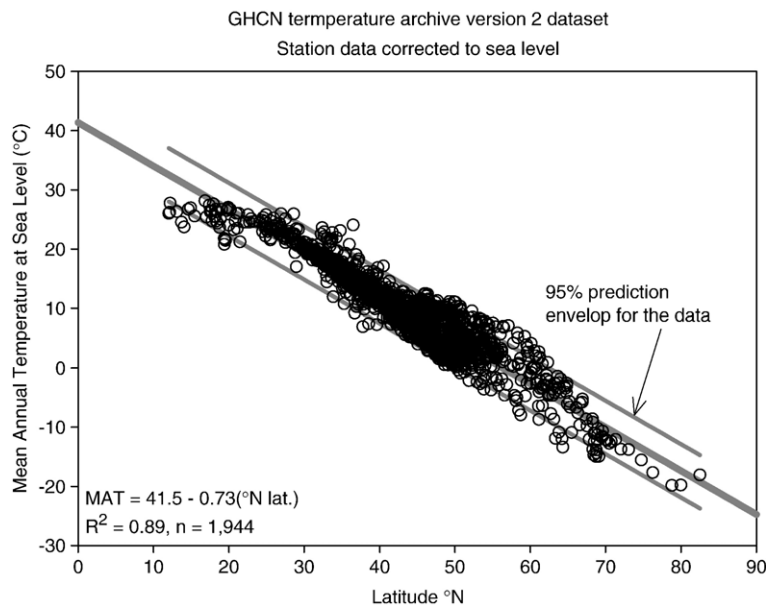


Fig. 4. Sea-level corrected *MAT* versus latitude for the 1944 stations in Fig. 3B. The best-fit line is reported in the text. The envelope around the line marks the 95% CI.

uncertainties for the calibration equation, which translate into larger uncertainties for an estimate of an unknown paleolatitude. However, this result depends on calibration samples that span the interior of NA from west to east and south to north, so that the zonal variation is represented in the calibration dataset.

For comparison, we used leaf-estimated MAT and P_i from the modern floral dataset (Fig. 2) to estimate the modern meridional thermal gradient (Fig. 5A and B) (see data repository for graphs of the confidence intervals). In this case, we used only those modern samples from the

northern hemisphere temperate zone at elevations less than 250 m (Table A2 in Appendix A). MAT_i and $SE[MAT_i]$ were estimated using (6b) and the algorithm in Appendix A. The meridional MAT profile was estimated using a weighted least-squares solution for (7) with b_2 held fixed at 0. The results are $b_0 = 42.9 \pm 3.57$ and $b_1 = -0.790 \pm 0.0918$ (± 1 SE), with $R^2 = 0.76$. The fit has $\chi^2_r = 0.7573$ and $P(\chi^2) = 79\%$, indicating that the residuals are not significantly different from those predicted by $SE[MAT_i]$. The meridional profile estimated from modern leaves is nearly identical to that estimated

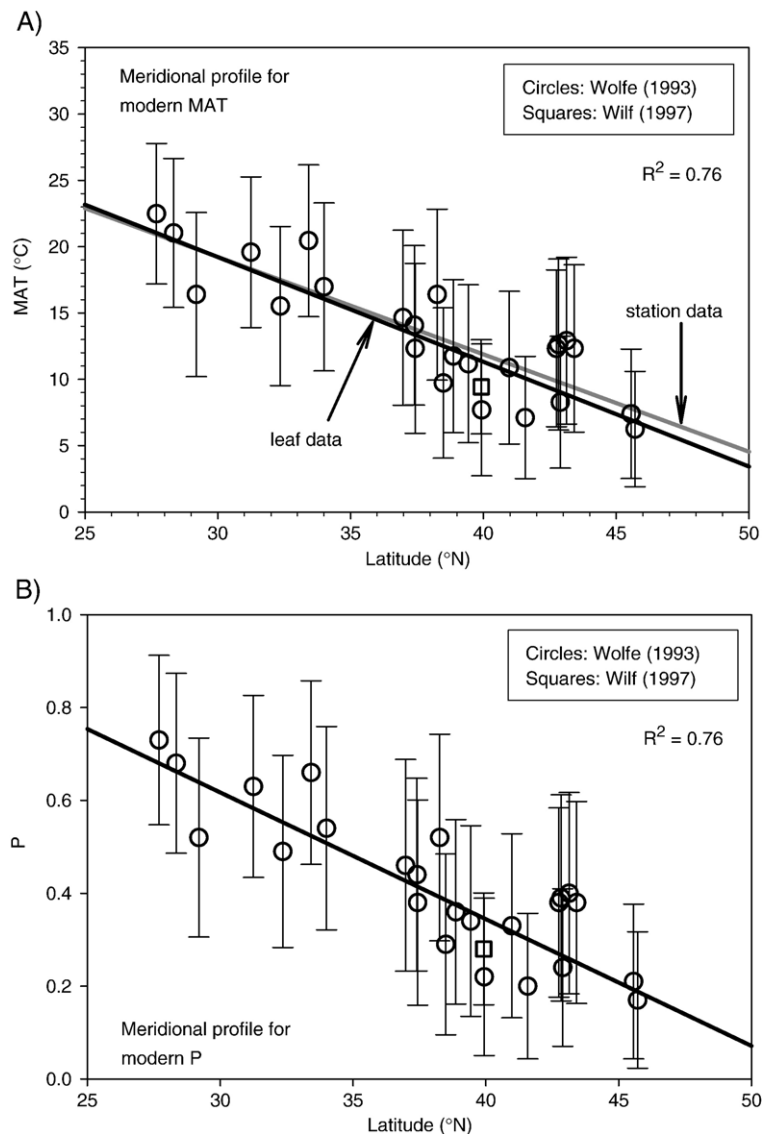


Fig. 5. (A) Estimate of MAT (error bars are 95% CI) as a function of latitude using modern leaf samples from compilation in Fig. 2. The analysis is restricted to those North American samples north of the tropics at elevations <250 m. The best-fit line is shown in black (see text). Gray line shows best-fit from MAT station data in Fig. 4. (B) Estimate of P (error bars are 95% CI) as a function of latitude using the same low-elevation modern floral sites in (A). The correlations demonstrate the feasibility of estimating latitude using leaf-margin data.

directly from station data (grey line Fig. 5A). This comparison may seem circular, but the station data used to estimate modern *MAT* values are almost entirely independent of the station data used to calibrate the relationship between *P* and *MAT* in Fig. 2A.

4. Modern *P* and latitude

We have shown that, in the temperate zone, *MAT* has a linear relationship with latitude (Fig. 4). Likewise, *P* has a linear relationship with *MAT* (Fig. 2). Thus, *P*

should be linearly related to latitude as shown in Fig. 5B. As a result, we can establish a calibration equation that relates *P* directly to latitude. This approach is tested using the modern low-elevation floral sites (Table A2 in Appendix A). The fit equation is

$$P = c_0 + c_1\lambda. \quad (8)$$

Weighted least-squares give $c_0 = 1.436 \pm 0.1234$ and $c_1 = -0.0273 \pm 0.0032$ (± 1 SE), with $R^2 = 0.76$. The fit has $X^2_r = 0.763$ and $P(\chi^2) = 78\%$, which indicates that the

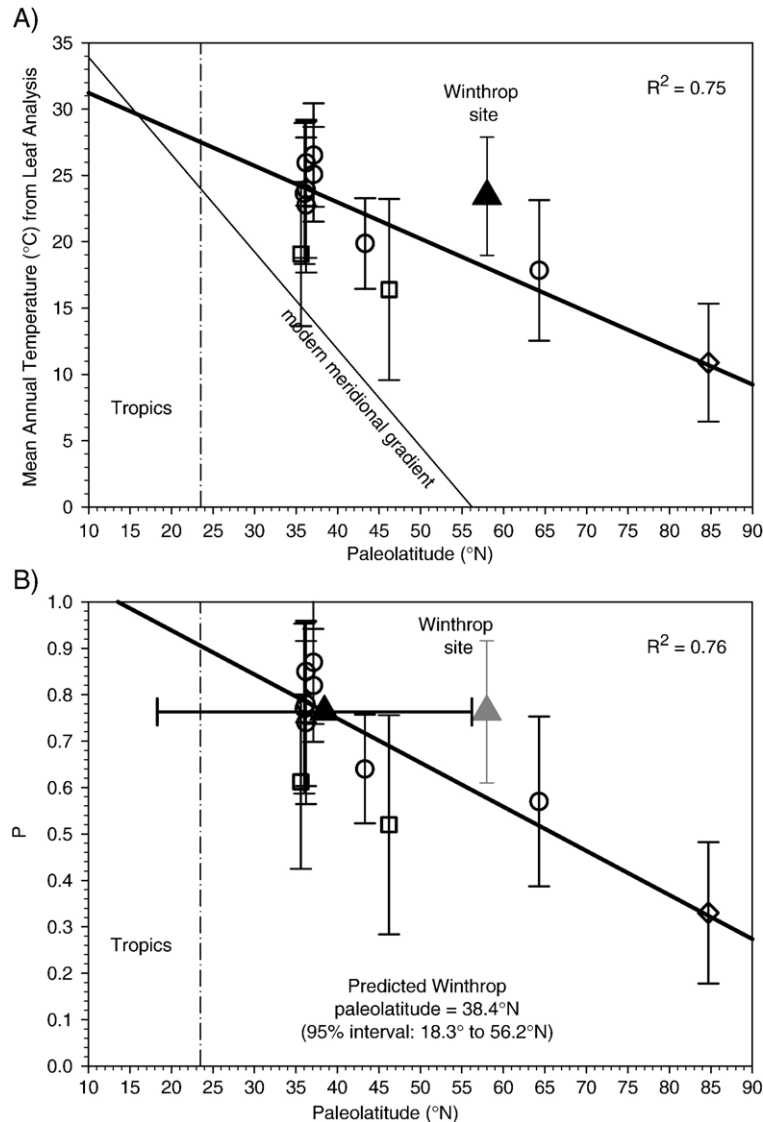


Fig. 6. Mid-Cretaceous meridional reference profile of (A) *MAT* and (B) *P* for stable NA estimated using 11 floral sites in Table 2. Symbols indicate age of the site: square: Albian, circle: Cenomanian, and diamond: undifferentiated Albian or Cenomanian. Error bars are 95% CI. Gray triangles show *MAT* and *P* for the Winthrop site as a function of expected-NA paleolatitude. Black triangle in (B) indicates the predicted paleolatitude for the Winthrop site. Best-fit lines are shown in black. The grey-line in (A) shows the modern *MAT* profile.

residuals are comparable to those predicted by $SE[P_i]$. Using the algorithm in Appendix A, we find that the 95% CI indicates that this calibration is able to estimate an unknown λ' to better than $\pm 7^\circ$, similar to the precision of latitudinal estimates provided by paleomagnetic studies.

5. P and paleolatitude for mid-Cretaceous North America

Leaf-margin data from 11 mid-Cretaceous (Albian and Cenomanian) sites in stable NA were compiled from [40,59–61] (Table 1). All sites lie east of the Rocky Mountain Trench, which is considered to be the western boundary of the stable interior of the NA plate. All floras grew near sea level based on coeval marine sediments found close by. Paleolatitude for each floral site was calculated using the mid-Cretaceous NA pole of Housen et al. [6] (70.1°N , 191.2°E , $A_{95}=2.7^\circ$). MAT and $SE[MAT]$ were estimated using Eqs. (6a) and (6b) and the algorithm in Appendix A. These samples were used to estimate mid-Cretaceous meridional reference profiles for MAT and P for stable NA. The reference profiles were then used to estimate the paleolatitude of the mid-to Late Albian Winthrop floral site, which is located in the east side of the Baja BC block (e.g., [62]).

The mid-Cretaceous meridional MAT profile was estimated (Fig. 6A) with a weighted least-squares solution for Eq. (7) with b_2 fixed to zero. The result is $b_0=34.0\pm 2.41$ and $b_1=-0.275\pm 0.0522$ (± 1 SE), with $R^2=0.75$. The fit has $\chi_r^2=1.31$ and $P(\chi^2)=32\%$, indicating that the residuals are comparable to those predicted by $SE[MAT_i]$.

The modern meridional profile is shown for comparison in Fig. 6A. Both profiles have similar MAT values in the tropics (at 20°N , the modern profile gives 26.9°C and the mid-Cretaceous profile, 28.5°C), but the mid-Cretaceous meridional gradient is only 40% of the modern gradient (0.28 vs. $0.73^\circ\text{C}/^\circ\text{latitude}$).

The calibration between λ and P was determined by weighted least-squares using Eq. (8) (Fig. 6B). The results are $b_0=1.129\pm 0.083$ and $b_1=-0.0095\pm 0.0018$ (± 1 SE) with $R^2=0.76$. The fit has $\chi_r^2=1.33$ and $P(\chi^2)=22\%$, indicating that the residuals are comparable to those predicted by $SE[P_i]$.

Ideally, we would like to have all fossil floral sites used to create our NA reference profile to be of exactly the same age as the Winthrop flora. Instead, the ages of the NA sites probably vary about $+5/-10$ Ma relative to ~ 105 Ma age of the Winthrop. Thus, we have focused on assembling a large number of sites near in age to the Winthrop flora in order to provide a good sample of the mean and variance for meridional MAT at that time. This approach is similar to that used in paleomagnetism to average the natural secular variation in the Earth's magnetic field. If we have adequately sampled the variation, then our inability to get exactly coeval MAT measurements is compensated by an increase in the uncertainties in our final result. For example, the Late Cenomanian is thought to have been usually warm [53]. We do not see any significant variation in the Albian and Cenomanian data used for our NA reference profile, other than that related to measurement errors in P_i . This result means that either our reference sites did not

Table 2
Mid-Cretaceous floral assemblages for stable NA and the Winthrop Formation

Assemblage [ref.]	Formation	Age	Lat. ($^\circ\text{N}$)	n	P	$2SE[P]$	MAT ($^\circ\text{C}$)	$2SE[MAT]$
<i>Sites from stable North America</i>								
1) Redmond [60]	Redmond	Albian	46.2	23	0.52	0.2362	16.4	6.8
2) Potomac [61]	Potomac	Albian	35.6	40	0.61	0.1875	19.1	5.4
3) Chandler [59]	Chandler	Albian or Cenom.	84.7	67	0.33	0.1524	10.9	4.4
4) Dunvegan [40]	Dunvegan	Cenom.	64.3	46	0.57	0.1831	17.8	5.3
5) Dakota [40]	Dakota	Cenom.	43.3	343	0.64	0.1170	19.9	3.4
6) Arthur Bluff [40]	Woodbine	Cenom.	37.1	30	0.87	0.1329	26.5	3.9
7) Denton Co. [40]	Woodbine	Cenom.	37.1	57	0.82	0.1217	25.1	3.6
8) Milton [40]	Raritan	Cenom.	36.2	27	0.78	0.1770	23.9	5.1
9) Woodbridge [40]	Raritan	Cenom.	36.2	59	0.85	0.1094	26.0	3.2
10) South Amboy [40]	Raritan	Cenom.	36.2	33	0.74	0.1755	22.8	5.1
11) Malden Mtn. [40]	Patapsco	Cenom.	36.0	26	0.77	0.1831	23.6	5.3
<i>Site from Baja BC block</i>								
Winthrop flora	Winthrop	Albian	58.6	43	0.76	0.1532	23.4	4.5

Abbreviations: ref. = citation reference; Cenom. = Cenomanian; Lat. ($^\circ\text{N}$) = paleolatitude, degrees north determined by 90 Ma NA pole from Housen et al. [6]; MAT = mean annual estimated from P .

sample the Late Cenomanian warming event, or that the magnitude of that warming event was small relative to the intrinsic precision of our *MAT* measurements.

6. Leaf data from the Winthrop Formation

The Winthrop Formation was deposited in the Methow/Tyaughton foredeep basin, which formed during the accretion of the Insular superterrane to NA at about 105 to 85 Ma [63,64]. The Methow basin corresponds to the southern half of this elongate basin. The Methow section begins with marine sediments, followed by fluvial sediments, and then ends with volcanic deposits. We focus here on the fluvial Winthrop

Formation, which hosts the floral deposits used in our study.

The Winthrop is a siliciclastic fluvio-deltaic unit [65], dominated by thick channelized beds of medium to very coarse arkosic sandstone with thin interbeds of silt or very fine sand, and local intervals of matrix-supported conglomerate. All parts of the unit contain compression–impression plant fossils of varying preservation quality. Interspersed in the arkosic beds are poorly defined, incipient paleosols. The most productive fossil-bearing beds are fine-grained, well-bedded over-bank deposits.

The Winthrop unconformably overlies the Harts Pass Formation, which contains mid-Albian ammonites



Fig. 7. Illustration of 43 dicotyledonous angiosperm species recognized from ~2500 leaf compression–impression fossils collected from the Winthrop Formation. Each sketch is a composite representation, commonly based on many individual fossils. Dotted lines appear where the species could not be fully reconstructed. The species are distinguished here using an informal numbering scheme; museum accession numbers are provided in Table A3 in Appendix A. Work in progress will provide a formal taxonomical analysis, but this level of detail is not needed for estimation of *P*. The species are divided into those with smooth margins (1–32) and those with serrated or toothed margins (33–43 see inset box). A fossil leaf is defined to have a “toothed margin” where the margin is broken by indentations that extend no more than 25% of the distance into the leaf towards the midrib or long axis of the leaf [90]. The toothed structure is commonly difficult to see in this illustration due to the reduced size of the sketches. Note that one species, #39, includes fossils with toothed margins and smooth margins, so it was classified as transitional with a score of 0.5. The *P* for the Winthrop assemblage is 0.76, which is based on 10.5 species with teeth and 32.5 without.

([66], R.A. Haugerud, pers. commun., 2004). The megafloral assemblage of the Winthrop correlates to the flora of upper subzone IIB in the Potomac Formation, which has been dated as mid-Albian (~110–105 Ma) [68]. Especially important to assigning this age is the high diversity of *Sapindopsis* species (14, 29, 38, and 39 in Fig. 7), which, in our experience, requires an age no younger than late Albian (>100 Ma). The Winthrop is cut by a dike, which has a U/Pb zircon age of 97.5^{+2}_{-3} Ma ([69], as cited in [70]). As a result, we assign a mid- to Late Albian age (110 to 100 Ma) to the Winthrop Formation.

Three field seasons of quarrying in the Winthrop Formation has produced a collection containing more than 2500 identifiable plant specimens. The flora is very diverse and includes bryophytes, horsetails, ferns, cycads, bennettites, conifers, and angiosperms, many of which represent new species. Our specimens are archived at the Denver Museum of Nature and Science, the Yale Peabody Museum, and the Burke Museum at the University of Washington. We also consulted a collection at the Smithsonian Institution that was made by I.C. Russell in 1896.

The flora was sorted into morphospecies, which are the finest category of entities that can be recognized and circumscribed as forming discrete populations within a fossil assemblage. We have found 43 dicotyledonous leaf species with leaf margins well enough preserved for identification and scoring (Fig. 7). The assemblage has $P=0.763\pm 0.077$ (± 1 SE), which gives an estimated MAT of 23.4 °C (± 1 SE=21.2° to 25.7 °C) and an estimated paleolatitude of 38.4°N (95% CI=18.3°N to 56.2°N) (Fig. 6B). The expected paleolatitude for the Winthrop Formation, if it had not moved relative to stable NA, is 58.6°N. The amount of northward offset relative to NA is given by the difference between the estimated paleolatitude and the expected-NA paleolatitude. The northward offset is 2240 km, with a 95% CI of 270 to 4470 km.

7. Discussion

The P value for the Winthrop flora indicates that it grew in a subtropical to tropical climate [38]. This conclusion is supported by other aspects of this flora. In particular, the sizes of the angiosperm leaves in Winthrop flora are anomalously large relative to those found in modern temperate forests (see species #10, 20 and especially 28 in Fig. 7). About 70% of the species have at least some specimens falling in the mesophyll-size class [see Ref. 71 for size-class definitions]. The only modern equivalents are tropical rainforests and

tropical seasonal forests where ~70% to 90% of leaves are mesophylls [72]. Several species exhibit a deeply cordate base, which is a morphology typical of vines (see species #2, 16, 37 and others in Fig. 7) and indicative of a tropical forest guild structure [73]. The Winthrop flora also exhibits a high diversity of both angiosperms and ferns, which is characteristic of modern tropical forests. Finally, modern tropical forests are the primary refugia for relict or nearly extinct taxa. Triassic and Jurassic relicts occur in the Winthrop flora; most notably, *Neocalamites*, which is globally widespread into the Early Jurassic but becomes endemic after that time. By the mid-Cretaceous, it is found in North America at only one location in NE Mexico [74,75]. Thus, the low paleolatitude estimated by our analysis is strongly supported by this more comprehensive consideration of the floristic characteristics of the Winthrop assemblage.

We now focus on the important constraint that the California sector provides on restoration of the Baja BC block. Our objective is to use this constraint, together with the Winthrop paleolatitude estimate, to determine probabilities for competing restorations for the Baja BC block (e.g., Fig. 1C and D). The California sector consists of four tectonostratigraphic units that are arranged in parallel belts within the western NA Cordillera (Fig. 1A). From east to west, these are: 1) the *pre-Cretaceous Klamath and Sierran terranes*, which are Paleozoic and early Mesozoic oceanic terranes that were accreted to NA during the Jurassic; 2) the *Cretaceous magmatic arc*, representing the Mesozoic “Andean-style” arc of NA, with the Sierra Nevada batholith as the type example; 3) the *Great Valley Group*, which is the Late Jurassic–Early Cenozoic forearc basin that formed outboard of the Sierra Nevada batholith; and 4) the *Franciscan Complex*, representing the coeval subduction complex that formed in association with the Sierran arc and the Great Valley basin.

Western Washington and southwestern British Columbia include tectonostratigraphic units that are fully equivalent to those in the California sector. They are found there in the large Late Cretaceous thrust nappes of the Coast Mountains orogen (yellow unit in Fig. 1), which marks the suture zone that formed when the Insular superterrane was accreted to NA between 100 and 85 Ma. Cowan et al. [1] used this observation to conclude that the Insular superterrane collided with an extension of the Franciscan–Great Valley–Sierran subduction zone, either to the south or to the north of the California sector. The restorations in Fig. 1C and D show that the Franciscan and Great Valley stop at the southern end of the California sector, whereas the 90 Ma

magmatic arc extends at least 1600 km farther to the south. The Cretaceous forearc appears to be missing in this area. This break may represent a truncation scar, where the Baja BC block was derived. This idea would account for occurrence of Franciscan and Great Valley rocks in the Coast Mountain orogen [76,77]. Conversely, one might argue that the Franciscan and Great Valley in the Coast Mountains orogen represents a natural northward continuation of these units from the Klamath Mountains. Garver [77] argues, based on detailed stratigraphic comparisons, that the southern location is more likely.

Our paleofloral evidence has considerable bearing on evaluating competing options for the original location of the Baja BC block. The cumulative probability curve in Fig. 8 is based on the probability distribution for our estimate of paleolatitude for the Winthrop flora. The

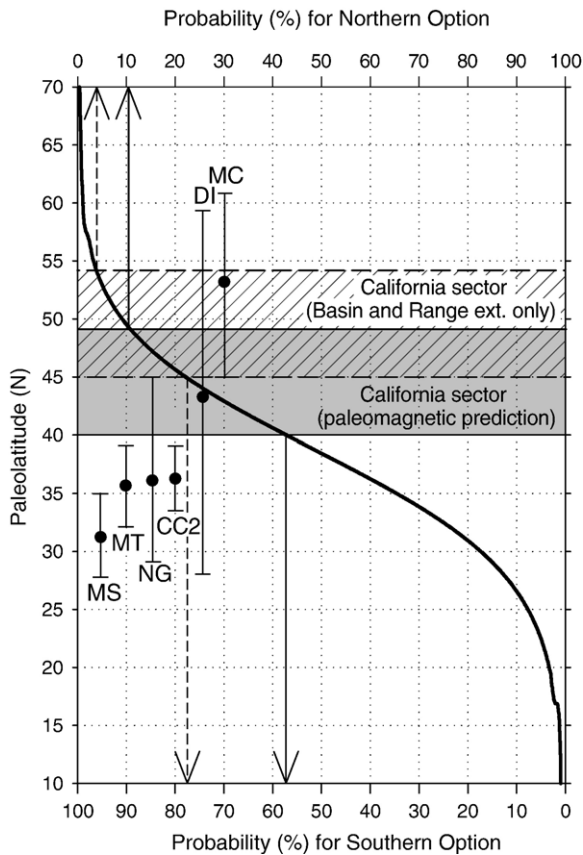


Fig. 8. Comparison of the Winthrop flora result with the Southern and Northern Options of Baja BC. The solid curve shows the cumulative probability for the predicted paleolatitude of the Winthrop flora at ~105 Ma (e.g., the most likely latitude indicated by the Winthrop flora is 38.4°N, which lies at 50% probability). The probability curve was calculated using the method for predicting error presented in Appendix A. For comparison, we include the paleomagnetic sites for Baja BC listed in Table 1. Error bars are shown at the 95% CI level.

gray and cross-hatched areas indicate the two possible mid-Cretaceous restorations for the California sector. The gray area shows the California sector 650 km south of its expected-NA location, as indicated by SN in Table 1. It is this version that is shown in Fig. 1C and D. An alternative is to restore the California sector southward by only 100 to 130 km, which accounts for the northward transport relative to NA caused by Basin-and-Range extension, as shown in Fig. 1B.

The cumulative probability for the Winthrop paleolatitude estimate can be used to calculate the probability that the Winthrop Formation originated north or south of the California sector. Consider first the paleomagnetically determined option for the California sector. The probability curve indicates that 58% of paleolatitudinal possibilities for the Winthrop Formation lie to the south, whereas only 10% lie north of the California sector. Now consider the California sector restored for Basin-and-Range extension alone. The probability curve indicates that 78% of the paleolatitudinal possibilities for the Winthrop lie south of the California sector, and 4% lie to the north. For comparison, we show the paleolatitude estimates for the main paleomagnetic sites from the Baja BC block (MS, MT, DI, NG, CC2 and MC in Table 1). The Duke Island site is ambiguous because of its large uncertainties. The MacColl Ridge site favors a Northern Option, but we agree with Mynatt et al. [20] that the young magnetization age for this site (~79 Ma) may mean that it did not record the full offset of the Baja BC block. The remaining four sites show good agreement with the Winthrop paleolatitude estimate. Collectively, they seem to strongly favor a Southern Option for the origin of the Baja BC block.

In the Introduction, we summarized the “yo-yo” interpretation of [13,25]. This idea requires that the mid-Cretaceous collision of the Insular superterrane occurred north of the California sector and that the new amalgamated collision zone was translated southward at ~100 Ma and then back north to its final location in the Cordilleran margin by 50 Ma. This interpretation is in direct conflict with our result for the Winthrop flora, which indicates a low paleolatitude for Baja BC in the mid- to late Albian (~110 to 100 Ma). At present, we see only three possibilities for resolving this conflict: 1) our Winthrop estimate may be flawed, 2) the paleomagnetic result for the Albian volcanic rocks of Churn Creek may be flawed, or 3) the contact between the conglomerates and volcanics at Churn Creek might be a major fault rather than a depositional contact. If the third option is correct, then the fault would mark a young tectonic boundary formed by the final docking of Baja BC against Alta BC. In other words the conglomerates

of Churn Creek would be part of the Baja BC block, equivalent to sediments in the Methow/Tyauhton basin, whereas the Albian volcanics of Churn Creek would be equivalent to the Spences Bridge Volcanics found to the east in Alta BC.

More work is needed to resolve this issue. Nonetheless, the conflict highlights the need for estimates for paleolatitude for the Baja BC block prior to 90 Ma. The Duke Island (DI) site has a magnetization age of 110 Ma, but it lacks the precision to resolve the conflict.

Our work also demonstrates the potential for using temperature measurements to estimate paleolatitude. Leaf-margin analysis is one way to make the necessary temperature measurements. However, geochemical methods may provide a faster and more precise method for measuring terrestrial surface temperatures and estimating paleolatitude.

8. Conclusion

The objective of this paper is to develop and apply a method using fossil leaves to quantitatively estimate paleolatitude. We start with a revised calibration of the prediction equation for estimation of *MAT* from measurements *P*. This analysis includes a more realistic assessment of the uncertainties for *MAT* estimates. We then show a strong correlation between *P*, *MAT*, and latitude for modern NA. Finally, we apply our method to estimate the paleolatitude of the Baja BC block. Extensive collections of fossil leaves from the Albian (110–100 Ma) Winthrop flora in the Methow basin yield a *P* value of 0.76. Using a paleolatitudinal reference profile of *P* determined from 11 Albian–Cenomanian floral sites from stable NA, we determine that the Winthrop flora originated at 38.4°N. This result provides independent support for a far-traveled Baja BC block, originating south of the California sector at ~105 Ma.

Acknowledgements

Numerous people and institutions have been involved in this study. Kirk Johnson and museum volunteers at the Denver Museum of Nature and Science helped during the first year of this project. Help and support during later years came from Linda Klise and volunteers at the Peabody Museum, Wesley Wehr at the University of Washington Burke Museum, and Scott Wing and Jon Wingeroth at the Smithsonian Institution. We are thankful for detailed discussions with Darrel Cowan (University of Washington), John Garver (Union College), Ted Irving (Geological Survey of Canada),

Ralph Haugerud (USGS), Bernie Housen (Western Washington University), Steven Sherwood (Yale), Lisa Tauxe (Scripps), and Peter Wilf (Penn State). We benefited from the critical reviews from Bernie Housen and an anonymous reviewer. We also thank Richard Beyer for logistical assistance and the Miller family for hard work on the outcrop. Miller's field work was supported by two GSA student research grants, a Sigma Xi research grant, and a YIBS Field Ecology grant. The Peabody Museum and Denver Museum of Nature and Science contributed shipping costs and curation of the samples.

Appendix A. Supplementary data

Supplementary data associated with this article can be found, in the online version, at [doi:10.1016/j.epsl.2006.02.022](https://doi.org/10.1016/j.epsl.2006.02.022).

References

- [1] D.S. Cowan, M.T. Brandon, J.I. Garver, Geologic tests of hypotheses for large coastwise displacements—a critique illustrated by the Baja British Columbia controversy, *Am. J. Sci.* 297 (1997) 117–173.
- [2] H. Gabrielse, Major dextral transcurrent displacements along the Northern Rocky Mountain Trench and related lineaments in north-central British Columbia, *Geol. Soc. Amer. Bull.* 96 (1985) 1–14.
- [3] R.A. Price, D.M. Carmichael, Geometric test for Late Cretaceous–Paleogene intracontinental transform faulting in the Canadian Cordillera, *Geology* 14 (1986) 468–471.
- [4] M.E.J. Beck, L. Nosen, Anomalous paleolatitudes in Cretaceous granitic rocks, *Nature* 235 (1972) 11–13.
- [5] J.J. Ague, M.T. Brandon, Regional tilt of the Mt. Stuart batholith, Washington, determined using Al-in-hornblende barometry: implications for northward translation of Baja British Columbia, *Geol. Soc. Amer. Bull.* 108 (1996) 471–488.
- [6] B.A. Housen, M.E. Beck Jr., R.F. Burmester, T. Fawcett, P. Petro, R. Sargent, K. Addis, K. Curtis, J. Ladd, N. Liner, B. Molitor, T. Montgomery, I. Mynatt, B. Palmer, D. Tucker, I. White, Paleomagnetism of the Mount Stuart batholith revisited again: what has been learned since 1972? *Am. J. Sci.* (2003) 263–299.
- [7] P.J. Wynne, E. Irving, J. Maxson, K.L. Kleinspehn, Paleomagnetism of the Upper Cretaceous strata of Mount Tatlow: evidence for 3000 km of northward displacement of the eastern Coast Belt, British Columbia, *J. Geophys. Res.* 100 (1995) 6073–6092.
- [8] E. Irving, P.J. Wynne, D.J. Thorkelson, P. Schiarizza, Large (1000 to 4000 km) northward movements of tectonic domains in the northern Cordillera, 83 to 45 Ma, *J. Geophys. Res.* 101 (1996) 17901–17916.
- [9] S.W. Bogue, C.S. Gromme, Structural correction of paleomagnetic vectors dispersed about two fold axes and application to the Duke Island (Alaska) ultramafic complex, *J. Geophys. Res.* 109 (2004) 1–13.
- [10] P.D. Ward, J.M. Hurtado, J.L. Kirschvink, K.L. Verosub, Measurements of the Cretaceous paleolatitude of Vancouver

- Island: consistent with the Baja-British Columbia hypothesis, *Science* 277 (1997) 1642–1645.
- [11] R.J. Enkin, J. Randolph, J. Baker, P.S. Mustard, Paleomagnetism of the Upper Cretaceous Nanaimo Group, southwestern Canadian Cordillera, *Can. J. Earth Sci.* 38 (2001) 1403–1422.
- [12] W. Krijgsman, L. Tauxe, E/I corrected paleolatitudes from the sedimentary rocks of the Baja British Columbia hypothesis, *Earth Planet. Sci. Lett.* 242 (2006) 205–216.
- [13] R.J. Enkin, J.B. Mahoney, J. Baker, J. Riesterer, M.L. Haskin, Deciphering shallow paleomagnetic inclinations: 2. Implications from Late Cretaceous strata overlapping the Insular/Intermontane Superterrane boundary in the southern Canadian Cordillera, *J. Geophys. Res.* 108 (2003), doi:10.1029/2002JB001983.
- [14] J.W.H. Monger, R.A. Price, in: P.J. Wynne, et al., (Eds.), Comment on: “Paleomagnetism of the Upper Cretaceous strata of Mount Tatlow: evidence for 3000 km of northward displacement of the eastern Coast Belt, British Columbia”, 1995; J.W.H. Monger, R.A. Price, in: E. Irving, et al., (Eds.), Paleomagnetism of the Spences Bridge Group and northward displacement of the Intermontane Belt, British Columbia: a second look, 1995; J.W.H. Monger, R.A. Price, *J. Geophys. Res.* 101 (1996).
- [15] P.J. Wynne, D.J. Thorkelson, K.L. Kleinspehn, J.A. Maxon, E. Irving, in: P.J. Wynne, et al., (Eds.), Reply to: Comment on ‘Paleomagnetism of the Upper Cretaceous strata of Mount Tatlow’, 1995; P.J. Wynne, D.J. Thorkelson, K.L. Kleinspehn, J.A. Maxon, E. Irving, in: E. Irving, et al., (Eds.), Paleomagnetism of the Spences Bridge Group and northward displacement of the Intermontane Belt, British Columbia: a second look, 1995; J.W.H. Monger, R.A. Price (Eds.), *Journal of Geophysical Research*, vol. 101, 1996, pp. 13801–13804.
- [16] R.F. Butler, G.E. Gehrels, K.P. Kodama, A moderate translation alternative to the Baja British Columbia hypothesis, *GSA Today* 11 (2001) 4–10.
- [17] B. Kim, K.P. Kodama, A compaction correction for the paleomagnetism of the Nanaimo Group sedimentary rocks: implications for the Baja British Columbia hypothesis, *J. Geophys. Res.* (2004), doi:10.1029/2003JB002696.
- [18] K.P. Kodama, P.D. Ward, Compaction-corrected paleomagnetic paleolatitudes for Late Cretaceous rudists along the Cretaceous California margin: evidence for less the 1500 km of post-Late Cretaceous offset for Baja British Columbia, *Geol. Soc. Amer. Bull.* 113 (2001) 1171–1178.
- [19] J.A. Stamatakos, J.M. Trop, K.D. Ridgway, Late Cretaceous paleogeography of Wrangellia: paleomagnetism of the MacColl Ridge Formation, southern Alaska, revisited, *Geology* 29 (2001) 947–950.
- [20] I. Mynatt, B.A. Housen, M.E. Beck Jr., in: J.A. Stamatakos, et al., (Eds.), Comment on: “Late Cretaceous paleogeography of Wrangellia: paleomagnetism of the McColl Ridge Formation, southern Alaska, revisited”, 2001, Online Forum doi: 10.1130/0091-7613(2003)31<e13:LCPOWP>2.0.CO2 (2003).
- [21] E. Irving, D.J. Thorkelson, P.M. Wheadon, R.J. Enkin, Paleomagnetism of the Spences Bridge Group and northward displacement of the Intermontane Belt, British Columbia: a second look, *J. Geophys. Res.* 100 (1995) 6057–6071.
- [22] P.J. Umhoefer, A model for the North American Cordillera in the Early Cretaceous: tectonic escape related to arc collision of the Guerrero terrane and a change in North American plate motion, in: S.E. Johnson, S.R. Paterson, J.M. Fletcher, G.H. Girty, D.L. Kimbrough, A. Martin-Barajas (Eds.), *Tectonic Evolution of Northwestern Mexico and the Southwestern USA*, Spec. Pap.—Geol. Soc. Am. 374 (2003) 117–134.
- [23] J.B. Mahoney, C.J. Hickson, P. van der Heyden, J.A. Hunt, The Late Albian–Early Cenomanian Silverquick conglomerate, Gang Ranch area: evidence for active basin tectonism, Current Research, Part A, *Geol. Soc. Can.* 91-1A (1992) 249–260.
- [24] J.W. Riesterer, J.B. Mahoney, P.K. Link, The conglomerate of Churn Creek: Late Cretaceous basin evolution along the Insular–Intermontane superterrane boundary, southern British Columbia, *Can. J. Earth Sci.* 38 (2001) 59–73.
- [25] M.L. Haskin, R.J. Enkin, J.B. Mahoney, P.S. Mustard, J. Baker, Deciphering shallow paleomagnetic inclinations: 1. Implications from correlation of Albian volcanic rocks along the Insular/Intermontane Superterrane boundary in the southern Canadian Cordillera, *J. Geophys. Res.* 108 (2003), doi:10.1029/2002JB001982.
- [26] R.A. Kerr, How far did the west wander? *Science* 268 (1995) 635–637.
- [27] J.M. Trop, K.D. Ridgway, A.R. Sweet, P.W. Layer, Submarine fan deposystems and tectonics of a Late Cretaceous forearc basin along an accretionary convergent plate boundary, MacColl Ridge Formation, Wrangell Mountains, Alaska, *Can. J. Earth Sci.* 36 (1999) 433–457.
- [28] J.B. Mahoney, P.S. Mustard, J.W. Haggart, R.M. Friedman, M.C. Fanning, V.J. McNicoll, Archean zircons in Cretaceous strata of the western Canadian Cordillera: the “Baja BC” hypothesis fails a “crucial test”, *Geology* 27 (1999) 195–198.
- [29] B.A. Housen, M.E. Beck Jr., Testing terrane transport: an inclusive approach to the Baja BC controversy, *Geology* 27 (1999) 1143–1146.
- [30] K. DeGraaff-Surpless, J.B. Mahoney, J.L. Wooden, M.O. McWilliams, Lithofacies control in detrital zircon provenance studies: insights from the Cretaceous Methow basin, southern Canadian Cordillera, *Geol. Soc. Amer. Bull.* 115 (2003) 899–915.
- [31] L. Ferrari, G. Pasquarè, S. Venegas-Salgado, F. Romero-Rios, Geology of the western Mexican Volcanic Belt and adjacent Sierra Madre Occidental and Jalisco block, Spec. Pap.—Geol. Soc. Am. 334 (1999) 65–83.
- [32] D.L. Hartmann, *Global Physical Climatology*, Academic Press, San Diego, 1994, 411 pp.
- [33] C.E. Forest, J.A. Wolfe, P. Molnar, K.A. Emanuel, Paleoaltimetry incorporating atmospheric physics and botanical estimates of paleoclimate, *Geol. Soc. Amer. Bull.* 111 (1999) 497–511.
- [35] B.T. Otto-Bliesner, E.C. Brady, C. Shields, Late Cretaceous ocean: coupled simulations with the National Center for Atmospheric Research Climate System Model, *J. Geophys. Res.* 107 (2002) 11-1–11-14.
- [36] J.A. Wolfe, A method of obtaining climatic parameters from leaf assemblages, U.S.G.S. Prof. Pap. 1106 (1993) 1–37.
- [37] S.L. Wing, D.R. Greenwood, Fossils and fossil climate: the case for equable continental interiors in the Eocene, *Philos. Trans. R. Soc. Lond., B* 341 (1993) 243–252.
- [38] J.A. Wolfe, Temperature parameters of humid to mesic forests of eastern Asia and relation to forests of other regions of the northern hemisphere and Australasia, U.S.G.S. Prof. Pap. 1106 (1979) 1–37.
- [39] D.L. Royer, P. Wilf, Why do toothed leaves correlate with cold climates? Gas exchange at leaf margins provides new insights into a classic paleotemperature proxy. *Int. J. Plant Sci.* 167 (2006) 11–18.

- [40] J.A. Wolfe, G.R. Upchurch, North American nonmarine climates and vegetation during the Late Cretaceous, *Palaeogeogr. Palaeoclimatol. Palaeoecol.* 61 (1987) 33–77.
- [41] I.W. Bailey, E.W. Sinnott, A botanical index of Cretaceous and Tertiary climates, *Science* 41 (1915) 831–834.
- [42] J.A. Wolfe, Paleoclimate estimates from Tertiary leaf assemblages, *Annu. Rev. Earth Planet. Sci.* 2040 (1995) 1–71.
- [43] P. Wilf, When are leaves good thermometers? A new case for leaf margin analysis, *Paleobiology* 23 (1997) 373–390.
- [44] D.R. Greenwood, S.L. Wing, Eocene continental climates and latitudinal temperature gradients, *Geology* 23 (1995) 1044–1048.
- [45] P. Wilf, K.R. Johnson, B.T. Huber, Correlated terrestrial and marine evidence for global climate changes before mass extinction at the Cretaceous–Paleogene boundary, *Proc. Natl. Acad. Sci. U. S. A.* 100 (2003) 599–604.
- [46] P. McCullagh, J.A. Nelder, *Generalized Linear Models*, Chapman and Hall, London, 1989, 511 pp.
- [47] J. Hinde, C.G.B. Demetrio, Overdispersion: models and estimation, *Comput. Stat. Data Anal.* 27 (1998) 151–170.
- [48] D.A. Williams, Extra-binomial variation in logistic linear models, *Appl. Stat.* 31 (1982) 144–148.
- [49] A. Agresti, *Categorical Data Analysis*, John Wiley & Sons, Hoboken, 2002, 710 pp.
- [50] R.J. Burnham, N. Pitman, K.R. Johnson, P. Wilf, Habitat-related error in estimating temperatures from leaf margins in a humid tropical forest, *Am. J. Bot.* 88 (2001) 1096–1102.
- [51] T.C. Peterson, R.S. Vose, An overview of the Global Historical Climatology Network temperature database, 2001, <http://lwf.ncdc.noaa.gov/oa/climate/research/ghcn/ghcnoverview.html> Data archive is at: <http://dss.ucar.edu/datasets/ds564.0/data/ver2/ghcnftp.html2001>.
- [52] R.D. Norris, K.L. Bice, E.A. Magno, P.A. Wilson, Jiggling the tropical thermostat in the Cretaceous hothouse, *Geology* 30 (2002) 299–302.
- [53] D.Z. Sun, Z. Liu, Dynamic ocean–atmosphere coupling: a thermostat for the tropics, *Science* 272 (1996) 1148–1150.
- [54] I.M. Held, A.Y. Hou, Nonlinear axially symmetric circulations in a nearly inviscid atmosphere, *J. Atmos. Sci.* 37 (1980) 515–533.
- [55] T.J. Crowley, J.C. Zachos, Comparison of zonal temperature profiles for past warm time periods, in: B.T. Huber, K.G. MacLeod, S.L. Wing (Eds.), *Warm Climates in Earth History*, Cambridge University Press, 2000.
- [56] S. Schouten, E.C. Hopmans, A. Forster, Y.v. Breugel, M.M. Kuypers, J.S. Damste, Extremely high sea-surface temperatures at low latitudes during the middle Cretaceous as revealed by archaeal membrane lipids, *Geology (Boulder)* 31 (2003) 1069–1072.
- [57] R. Seager, D.S. Battist, J. Yin, N. Gordon, N. Naik, A.C. Clement, M.A. Cane, Is the Gulf Stream responsible for Europe’s mild winters? *Q. J. R. Meteorol. Soc.* 128 (2002) 2563–2586.
- [58] J.T. Parrish, R.A. Spicer, Late Cretaceous terrestrial vegetation: a near-polar temperature curve, *Geology* 16 (1988) 22–25.
- [59] L.J. Hickey, T.B. Armstrong, A mid-Cretaceous (Cenomanian) Flora from the Interior of the Canadian Shield in Western Labrador, Annual Meeting, vol. 49 (26.8), American Institute of Biological Sciences, 1998.
- [60] L.J. Hickey, Potomac flora (unpublished data).
- [61] J.M. Journeay, R.M. Friedman, The Coast Belt thrust system: evidence for Late Cretaceous shortening in southwest British Columbia, *Tectonics* 12 (1993) 756–775.
- [62] M.E. Tennyson, M.R. Cole, Upper Mesozoic Methow–Pasayton sequence northeastern Cascade Range, Washington and British Columbia, Washington Division of Geology and Earth Resources Bulletin, vol. 77, 1987, pp. 73–84.
- [63] M.F. McGroder, Structural geometry and kinematic evolution of the eastern Cascades foldbelt, Washington and British Columbia, *Can. J. Earth Sci.* 26 (1989) 1586–1602.
- [64] R.L. Rau, Sedimentology of the Upper Cretaceous Winthrop Sandstone, Northeastern Cascade Range, Washington, Masters, Eastern Washington University, 1987, 196 pp.
- [65] B.E. Crowley, Early Cretaceous (Albian) Ammonites from the Harts Pass Formation, Methow Basin, Washington, Masters, University of Washington, 1993, 46 pp.
- [66] L.J. Hickey, J.A. Doyle, Early Cretaceous fossil evidence for angiosperm evolution, *Bot. Rev.* 43 (1977) 3–104.
- [67] R.A. Haugerud, J.B. Mahoney, J.D. Dragovich, Geology of the methow block, Northwest Geological Society Meeting, Northwest Geological Society, Seattle, WA, 1996.
- [68] R.J. Enkin, J.B. Mahoney, J. Baker, M. Kiessling, R.A. Haugerud, Syntectonic remagnetization in the southern Methow block: resolving large displacements in the southern Canadian Cordillera, *Tectonics* 21 (2002) 18-1–18-18.
- [69] C. Raunkiaer, *The Life Forms of Plants and Statistical Plant Geography*, Clarendon Press, Oxford, 1934, 632 pp.
- [70] P.W. Richards, *The Tropical Rain Forest: An Ecological Study*, Cambridge University Press, London, 1952, 450 pp.
- [71] T. Givnish, On the adaptive significance of leaf form, in: O.T. Solbrig, S. Jain, G.B. Johnson, P. Raven (Eds.), *Topics in Plant Population Biology*, Columbia University Press, 1979, pp. 375–407;
- [72] T. Givnish, G. Vermeij, Sizes and shapes of liane leaves, *Am. Nat.* 110 (1976) 743–778.
- [73] M.M. Koerdell, Nueva equisetel del Cretacico superior de Choahuila, Mexico, *Bull. Assoc. Mex. Pet. Geol.* 1 (1949) 27–34.
- [74] E. Boureau, Sphenophyta and Noeggerathiophyta, Masson, Paris, 1964, 1–544 pp.
- [75] M.T. Brandon, D.S. Cowan, J.A. Vance, The Late Cretaceous San Juan thrust system, San Juan Islands, Washington, *Spec. Pap.—Geol. Soc. Am.* 221 (1988) 1–81.
- [76] J.I. Garver, Fragment of the Coast Range ophiolite and the Great Valley sequence in the San Juan Islands, Washington, *Geology* 16 (1988) 948–951.
- [77] L.S. Frei, J.R. Magill, A. Cox, Paleomagnetic results from the central Sierra Nevada: constraints on reconstructions of the western United States, *Tectonics* 3 (1984) 157–177.
- [78] L.S. Frei, Additional paleomagnetic results from the Sierra Nevada: further constraints on Basin and Range extension and northward displacement in the western United States, *Geol. Soc. Amer. Bull.* 97 (1986) 840–849.
- [79] K.J. Whidden, S.P. Lund, D.J. Bottjer, D. Champion, D.G. Howell, Paleomagnetic evidence that the central block of Salinia (California) is not a far-traveled terrane, *Tectonics* 12 (1998) 329–343.
- [80] R.F. Teissere, M.E. Beck Jr., Divergent Cretaceous paleomagnetic pole position for the southern California batholith, USA, *Earth Planet. Sci. Lett.* 18 (1973) 296–300.
- [81] J.T. Hagstrum, M. McWilliams, D.G. Howell, C.S. Gromme, Mesozoic paleomagnetism and northward translation of the Baja California Peninsula, *Geol. Soc. Amer. Bull.* 96 (1985) 1077–1090.
- [82] J.J. Ague, M.T. Brandon, Tilt and northward offset of Cordilleran batholiths resolved using igneous barometry, *Nature* 360 (1992) 146–149.

- [84] K.C. Bayer, Generalized structural lithologic and physiographic provinces in the fold and thrust belts of the United States: exclusive of Alaska and Hawaii, U.S. Geological Survey, 1983.
- [85] N.J. Silberling, D.L. Jones, J.W.H. Monger, P.J. Coney, Lithotectonic Terrane Map of the North American Cordillera, U.S. Geological Survey, 1992.
- [86] R.L. Armstrong, P.L. Ward, Late Triassic to earliest Eocene magmatism in the North American Cordillera: implications for the Western Interior Basin, in: W.G.E. Caldwell, E.G. Kauffmann (Eds.), Evolution of the Western Interior Basin, Geological Association of Canada, vol. 39, 1993, pp. 49–72.
- [87] J.K. Snow, B. Wernicke, Cenozoic tectonism in the central Basin and Range; magnitude, rate, and distribution of upper crustal strain, *Am. J. Sci.* 300 (2000) 659–719.
- [88] P. Wessel, W.F. Smith, New, improved version of the Generic Mapping Tools released, *EOS, Trans.* 79 (1998) 579.
- [89] R.A. Spicer, <http://tabitha.open.ac.uk/spicer/CLAMP/Clampset1.html>2003, 2003.
- [90] Leaf Architecture Working Group, Manual of Leaf Architecture—Morphological Description and Categorization of Dicotyledonous and Net-Veined Monocotyledonous Angiosperms, 1999, 65 pp.

DATA REPOSITORY FOR MILLER ET AL. (2006)

INTRODUCTION

This data repository provides supporting information for Miller et al. (2006). Included here are:

- 1) The algorithm used to estimate the parameters for a calibration equation and for determining the uncertainties for predictions made with the calibration equation.
- 2) Table A1 lists modern leaf-margin data for low-elevation sites in temperate North America, which are also part of the modern calibration dataset for P versus MAT .
- 3) Table A2 lists the remaining leaf-margin data for the modern calibration dataset
- 4) Table A3 lists the museum accession numbers for the species drawn in Figure 8 of the paper.
- 5) The Matlab script used to generate the results in Table 2.
- 6) Figures A1 and A2 show details of the ability of the logistic normal variance function to handle the overdispersion in measurements of P , as represented by the modern calibration dataset.
- 7) List of references cited in this document.

UNCERTAINTIES FOR PREDICTIONS FROM CALIBRATION EQUATIONS

Our analysis above is based on the use of calibration equations to predict temperature and latitude. Here we summarize our calculations for estimating uncertainties for predictions determined from a calibration equation. We refer interested readers to Osborne (1991) for a comprehensive review of the statistical issues associated with calibration and prediction.

We focus on a linear two-parameter calibration equation, as used in this study. In this situation, we have N paired measurements, x_i and y_i , which are used to estimate a calibration equation. The equation is then used to predict unknown values of x' from measured values of y' . A common feature of many calibration problems is that the y measurements typically have larger errors than the x measurements. The two methods for calibration deal with these errors in different ways. The *classic calibration* method (Osborne 1991) specifies the calibration equation as

$$y_i = a_0 + a_1 x_i + \varepsilon_i. \quad (1)$$

The y variable is on the left side, given that the misfit in the calibration is attributed to errors ε_i in the y_i measurements. Least-squares regression is used to find a best-fit solution for the parameters a_0 and a_1 . At this point, we invert the equation

$$x' = (y' - a) / b, \quad (2)$$

so that we can use measurements of y' to predict x' .

The *inverse calibration* method (Osborne 1991) uses a reversed arrangement for the calibration equation where

$$x_i = b_0 + b_1 (y_i - \varepsilon_i) = b_0 + b_1 y_i - b_1 \varepsilon_i. \quad (3)$$

The regression analysis will find a solution that minimizes the misfit, but note that the errors associated with y_i are now convolved with the unknown parameter b_1 . This accounts for why inverse calibration will give a different best-fit line than the classical calibration method. The resulting calibration equation will provide reliable predictions,

$$x' = b_0 + b_1 y',$$

as long as the measurements for y' come from the same range and have the same distributional properties as the y_i values used to estimate the calibration (Chow and Shao 1990; Osborne 1991).

For our study here, we prefer the classical calibration method because it allows us to analyze the errors associated with y_i (which is P_i in our case). Draper and Smith (1998) summarize the calculation for estimating the confidence interval for a prediction of x' (Note that Draper and Smith (1998) create some confusion by referring to this calculation as “inverse least-squares”, when in fact it is associated with the classical calibration method.) We modify their calculation to account for our situation where $SE[y']$ is determined independent of the least-squares calibration.

The uncertainties in the estimates a_0 , a_1 , and y' all contribute to the uncertainty for the prediction x' . We seek values x_L and x_U that define a confidence interval around x' at a specified two-tail significance level indicated by the probability α . For example, a 95% CI would have $\alpha = 2.5\%$. First, we need to calculate the least-squared solution for the calibration equation. For a weighted solution, set the weights to $w_i = SE[y_i]^{-2}$. For an unweighted solution, set all of the weights w_i to one.

$$S_w = \sum w_i$$

$$S_{xx} = \sum w_i (x_i - \bar{x})^2$$

$$S_{yy} = \sum w_i (y_i - \bar{y})^2$$

$$S_{xy} = \sum w_i (x_i - \bar{x})(y_i - \bar{y})$$

$$\bar{x} = S_w^{-1} \sum w_i x_i$$

$$\bar{y} = S_w^{-1} \sum w_i y_i$$

$$a_1 = \frac{S_{xy}}{S_{xx}}$$

$$a_0 = \bar{y} - b\bar{x}$$

$$S_{ee} = S_{yy} - a_1^2 S_{xx}$$

$$SE[\bar{y}]^2 = \frac{S_{ee}}{(N-2)S_w}$$

$$SE[a_0]^2 = \frac{S_{ee}}{(N-2)} \left(S_w^{-1} + \frac{\bar{x}^2}{S_{xx}} \right)$$

$$SE[a_1]^2 = \frac{S_{ee}}{(N-2)S_{xx}}$$

$$R^2 = 1 - \frac{S_{ee}}{S_{yy}}$$

The confidence interval is defined by

$$\{x_U, x_L\} = \hat{x}_o + \frac{g(x' - \bar{x}) \pm a_1^{-1} \left[(t_1 SE(a_1)(x' - \bar{x}))^2 + (1-g) \left((t_1 SE[\bar{y}])^2 / N + (t_2 SE(y'))^2 \right) \right]^{1/2}}{1-g}$$

where $g = (t_1 SE[a_1]/a_1)^2$, and $SE[y']$ is the standard error for y' . The confidence interval

for uncertainties associated with the calibration equation alone is given by setting $SE[y']$

= 0. The variables t_1 and t_2 indicate the value for the t distribution given a probability P

and degrees of freedom ν . In particular, $t_1 = t(P = 1 - \alpha/2, \nu = N - 2)$ and

$t_2 = t(P = 1 - \alpha/2, \nu = \infty)$. Note that the confidence interval will be, in general,

asymmetric around x' . Setting $\alpha = 2.5\%$ gives the 95% CI and $\alpha = 16\%$ gives the 68%

CI, which provides an estimate for $SE[x']$.

Table A1. Low elevation temperate flora sites used shown in Figure 6. These data are also used in the modern calibration dataset (Figure 3). Elevations here are all less than 250 m. Locations are all in the temperate zone (north of 23.5°N). The sites are sorted in descending mean annual temperature (*MAT*). Data are from Wolfe (1993) and Wilf (1997).

<u>CLAMP Wolfe (1993)</u>	<u><i>MAT</i> °C</u>	<u><i>P</i></u>	<u><i>n</i></u>	<u>Elevation (m)</u>
Avon Park, Florida	22.4	0.73	31	30
Orlando, Florida	22.2	0.68	31	15
Lake George, Florida	21.0	0.52	30	5
Brunswick, Georgia	19.6	0.63	34	2
Beaufort, South Carolina	19.0	0.49	33	5
Simmons ville, South Carolina	17.8	0.66	31	5
Kure Beach, North Carolina	16.7	0.54	28	5
Camp Pardee, California	16.4	0.52	37	170
Jasper Ridge, California	14.7	0.44	32	30
Santa Cruz, California	13.9	0.46	25	2
S.I.E.R.C., Maryland	13.5	0.36	32	30
Battle Cr., Maryland	13.1	0.29	28	10
Half Moon Bay, California	12.6	0.38	25	10
Powers, Oregon	12.0	0.24	33	60
Troutdale, Oregon	12.0	0.21	30	10
Frederick, Maryland	11.7	0.34	28	100
Port Orford, Oregon	11.7	0.38	31	10
North Bend, Oregon	11.5	0.38	26	3
Arendtsville, Pennsylvania	11.2	0.22	30	220
Bandon, Oregon	11.0	0.40	27	2
Hood River, Oregon	10.3	0.17	32	170
Cape Blanco, Oregon	10.2	0.39	25	10
Stroudsburg, Pennsylvania	9.90	0.33	30	160
Tunkhannock, Pennsylvania	8.60	0.20	33	240
<u>Wilf (1997)</u>	<u><i>MAT</i> °C</u>	<u><i>P</i></u>	<u><i>n</i></u>	<u>Elevation (m)</u>
York County, Pennsylvania	11.8	0.28	132	118

Table A2. Remaining flora sites used in the modern calibration dataset (Figure 3). These sites are from North and Central America and include locations in both the tropics and the temperate zone. The sites are sorted by descending *MAT*. Elevations for the Wilf (1997) sites are included here. The elevations for the Wolfe (1993) sites are not included here, but are available in that source.

<i>CLAMP Wolfe (1993)</i>	<i>MAT</i> °C	<i>P</i>	<i>n</i>
Cabo Rojo, Puerto Rico	26.8	0.87	30
Guanica, Puerto Rico	26.8	0.83	33
Borinquen, Puerto Rico	25.5	0.83	41
Cambalache, Puerto Rico	25.5	0.87	37
Guajatica, Puerto Rico	24.8	0.72	38
Susua Alta, Puerto Rico	24.5	0.80	42
Buena Vista, Puerto Rico	22.0	0.81	38
Canyon Lake, Arizona	21.9	0.78	30
Maricao, Puerto Rico	21.7	0.81	35
Bartlett Resvr., Arizona	21.4	0.80	20
Castle Cr., Arizona	20.9	0.73	23
Saguaro Lake, Arizona	20.6	0.75	24
Superior, Arizona	20.4	0.69	29
Roosevelt Lk., Arizona	19.8	0.72	23
Monte Guilarte, Puerto Rico	19.0	0.76	33
Punkin Center, Arizona	18.0	0.75	30
Childs, Arizona	17.9	0.63	24
Toro Negro, Puerto Rico	17.9	0.69	44
Santa Rita, Arizona	17.8	0.64	28
Miami, Arizona	17.5	0.60	21
Auburn, California	15.7	0.48	29
Jerome, Arizona	15.3	0.46	26
Colfax, California	14.9	0.44	27
Sierra Ancha, Arizona	14.9	0.63	27
Yava, Arizona	14.9	0.60	24
Natural Bridge, Arizona	14.5	0.55	28
Canelo, Arizona	14.1	0.58	31
Lakeport, California	14.0	0.52	21
Placerville, California	13.9	0.25	24
Junipine, Arizona	13.1	0.32	27
Payson, Arizona	13.1	0.46	28
Prescott AP, Arizona	12.9	0.37	30
Kitt Peak, Arizona	12.8	0.50	23
Crown King, Arizona	12.1	0.44	25
Blue Canyon, California	10.3	0.37	23
Hasayampa, Arizona	10.2	0.27	22
Three Lynx, Oregon	10.0	0.18	30
Bowman Dam, California	9.5	0.40	31
Los Alamos, New Mexico	9.0	0.29	25

Wind River, Washington	8.9	0.21	30
Lake Spaulding, California	8.7	0.40	31
Parkdale, Oregon	8.5	0.23	35
Sierraville, California	8.0	0.32	30
Cheesman Resvr., Colorado	7.2	0.17	27
Mt. Pocono, Pennsylvania	7.2	0.17	28
River Falls, Wisconsin	7.0	0.16	22
Rimrock Lake, Washington	6.8	0.18	25
Dannemora, New York	6.5	0.13	30
Republic, Washington	6.1	0.20	28
Wanakena, New York	5.2	0.23	29
Lake Placid, New York	4.3	0.10	24

<u>Wilf (1997)</u>	<u>MAT °C</u>	<u>P</u>	<u>n</u>	<u>Elevation (m)</u>
Barro Colorado Island	27.1	0.80	629	150
Beni Biodiversity Plots	27.0	0.83	104	194
St. John, dry woodland	26.9	0.80	173	~200
St. John, moist forest	26.3	0.82	227	~200
Guanica Forest	25.1	0.86	126	~200
Bisley Watersheds	24.4	0.78	131	~500
Manu Biodiversity Plots	24.2	0.87	292	400
Allegheny National Forest	7.2	0.24	74	503

Table A3. Museum accession numbers for species illustrated in Figure 8. The list is formatted as follows: Museum acronym/name, specimen number, locality number (notation varies between institution). Museum abbreviations are as follows: DMNH = Denver Museum of Nature and Science; Burke = Burke Museum of Natural History and Culture; YPM = Yale Peabody Museum of Natural History; USNM = Smithsonian Institution National Museum of Natural History. Note that species that show multiple specimen numbers are composite drawings from several fossils.

1. DMNH #18968, loc. #2226
2. DMNH #18966, loc. #2226
3. DMNH #18963, loc. #2226; #18964, loc. #2226
4. DMNH #18991, loc. #2226
5. DMNH #18962, loc. #2226
6. DMNH #18961, loc. #2226; Burke #97300, loc. A4417
7. DMNH #18990, loc. #2227
8. DMNH #18972, loc. #2227
9. YPM #160820, loc. IM0215
10. DMNH #18969, #18970, loc. #2226
11. YPM #160822, loc. IM0201
12. YPM #160817, loc. IM0201
13. USNM #530286, loc. 2089
14. USNM #530287, loc. 2089
15. DMNH #18975, #18976, loc. #2226
16. DMNH #26007, loc. #2226
17. USNM #530285, loc. 1842
18. YPM #160824, loc. IM0215
19. Burke #97296, loc. #A4417
20. YPM #160810, #160811, loc. IM0201
21. YPM #160826, loc. IM0201
22. YPM #160812, loc. IM0203
23. DMNH #23233, loc. #2226
24. YPM #160821, loc. IM0201
25. YPM #160816, loc. IM0208
26. DMNH #18973, loc. #2226; #18974, loc. #2227
27. YPM #160827, loc. IM0210
28. USNM #530284, loc. 2089
29. Burke #97299, loc. #A4417
30. YPM #160813, loc. IM0208
31. YPM #160814, loc. IM0208
32. YPM #160823, loc. IM0215
33. DMNH #18979, loc. #2227
34. YPM #160818, loc. IM0201
35. YPM #160809, loc. IM02-2226; DMNH #18992, loc. #2226
36. YPM #160819, loc. IM02-2226
37. DMNH #18967, loc. #2226
38. DMNH #18982, loc. #2226

39. YPM #160815, loc. IM0205
40. YPM #160825, loc. IM02-2226
41. DMNH #25970, loc. #2226
42. Burke #97292, loc. #A4417
43. YPM #160828, loc. IM0210

MATLAB SCRIPT ILLUSTRATING ESTIMATION CALCULATIONS, AS USED TO GENERATE RESULTS SHOWN IN TABLE 2.

```

%=====
%... PredictMAT.m, Mark Brandon, Yale University, 2006
% This Matlab script provides a example of the calculations used for
% Miller et al. (EPSL, 2006). In this version, it estimates the
% calibration equation for P and MAT reported in Miller et al., and
% the prediction of MAT values and confidence limits for P values
% reported in Table 2 of Miller et al.
% The first part of this script shows the calibration analysis.
% The calibration dataset of 84 sites is included below.
% The second part of the script shows the use of the calibration
% equation for prediction of MAT and the estimation of
% confidence intervals for the MAT estimate.
% Script was written using Matlab version 7.1.

%...Confidence limits for prediction are modified from formulae in Smith and
% Draper, as outlined in the appendix in Miller et al.
%... SE(P) is given by the logistic normal variance function
%... Make sure that input values in this section are correctly assigned
%... x >> MAT
%... y >> P values for reference sites
%...nfory >> Number of species for each P value for reference sites

%... Load calibration data from Wolfe 1993 and Wilf 1997
MAT=[26.8 26.8 25.5 25.5 24.8 24.5 22.4 22.2 22.0 21.9 21.7 21.4 21.0 ...
    20.9 20.6 20.4 19.8 19.6 19.0 19.0 18.0 17.9 17.9 17.8 17.8 17.5 ...
    16.7 16.4 15.7 15.3 14.9 14.9 14.9 14.7 14.5 14.1 14.0 13.9 13.9 ...
    13.5 13.1 13.1 13.1 12.9 12.8 12.6 12.1 12.0 12.0 11.7 11.7 11.5 ...
    11.2 11.0 10.3 10.3 10.2 10.2 10.0 9.9 9.5 9.0 8.9 8.7 8.6 8.5 ...
    8.0 7.2 7.2 7.0 6.8 6.5 6.1 5.2 4.3 27.0 24.2 27.1 24.4 25.1 ...
    26.9 26.3 11.8 7.2]';
P=[0.83 0.87 0.83 0.87 0.72 0.80 0.73 0.68 0.81 0.78 0.81 0.80 0.52 ...
    0.73 0.75 0.69 0.72 0.63 0.76 0.49 0.75 0.69 0.63 0.66 0.64 0.60 ...
    0.54 0.52 0.48 0.46 0.63 0.44 0.60 0.44 0.55 0.58 0.52 0.46 0.25 ...
    0.36 0.29 0.32 0.46 0.37 0.50 0.38 0.44 0.24 0.21 0.38 0.34 0.38 ...
    0.22 0.40 0.17 0.37 0.39 0.27 0.18 0.33 0.40 0.29 0.21 0.40 0.20 ...
    0.23 0.32 0.17 0.17 0.16 0.18 0.13 0.20 0.23 0.10 0.832 0.872 ...
    0.797 0.782 0.864 0.795 0.822 0.28 0.243]';
nforP=[33 30 41 37 38 42 31 31 38 30 35 20 30 23 24 29 23 34 33 33 ...
    30 44 24 31 28 21 28 27 29 26 27 27 24 32 28 31 21 25 24 32 28 ...
    27 28 30 23 25 25 33 30 31 28 26 30 27 32 23 25 22 30 30 31 25 ...
    30 31 33 35 30 28 27 22 25 30 28 29 24 104 292 629 131 126 173 ...
    227 132 74]';
%... Index and Name give numbering and names as reported in the original
% Wolfe 1993 and Wilf 1997 references. These data are organized in the same
% manner as MAT, P, and n above. Index and Name are not used in the
% calculations below but are included here for completeness.
% Index=[1 2 6 7 10 11 20 21 23 25 27 29 31 32 34 35 36 37 40 41 42 ...
% 44 45 46 47 48 51 53 56 59 63 64 65 66 67 68 69 70 71 75 78 79 ...
% 80 82 83 84 88 90 91 95 96 98 100 101 105 106 107 108 110 111 ...
% 114 118 119 120 121 123 125 128 129 130 132 134 136 137 142 ...
% 1 2 3 4 5 6 7 8 9]';
% Name=['Guanica, Puerto Rico' 'Cabo Rojo, Puerto Rico' ...
% 'Borinquen, Puerto Rico' 'Cambalache, Puerto Rico' ...
% 'Guajatica, Puerto Rico' 'Susua Alta, Puerto Rico' ...
% 'Avon Park, Florida' 'Orlando, Florida' ...
% 'Buena Vista, Puerto Rico' 'Canyon Lake, Arizona' ...
% 'Maricao, Puerto Rico' 'Bartlett Resvr., Arizona' ...
% 'Lake George, Florida' 'Castle Cr., Arizona' ...
% 'Saguaro Lake, Arizona' 'Superior, Arizona' ...
% 'Roosevelt Lk., Arizona' 'Brunswick, Georgia' ...
% 'Monte Guilarte, Puerto Rico' 'Beaufort, South Carolina' ...
% 'Punkin Center, Arizona' 'Toro Negro, Puerto Rico' ...
% 'Childs, Arizona' 'Simmons ville, South Carolina' ...
% 'Santa Rita, Arizona' 'Miami, Arizona' 'Kure Beach, North Carolina' ...
% 'Camp Pardee, California' 'Auburn, California' 'Jerome, Arizona' ...
% 'Sierra Ancha, Arizona' 'Colfax, California' 'Yava, Arizona' ...
% 'Jasper Ridge, California' 'Natural Bridge, Arizona' 'Canelo, Arizona' ...
% 'Lakeport, California' 'Santa Cruz, California' 'Placerville, California' ...
% 'S.I.E.R.C., Maryland' 'Battle Cr., Maryland' 'Junipine, Arizona' ...
% 'Payson, Arizona' 'Prescott AP, Arizona' 'Kitt Peak, Arizona' ...
% 'Half Moon Bay, California' 'Crown King, Arizona' 'Powers, Oregon' ...
% 'Troutdale, Oregon' 'Port Orford, Oregon' 'Frederick, Maryland' ...
% 'North Bend, Oregon' 'Arendtsville, Pennsylvania' 'Bandon, Oregon' ...
% 'Hood River, Oregon' 'Blue Canyon, California' 'Cape Blanco, Oregon' ...
% 'Hasayampa, Arizona' 'Three Lynx, Oregon' 'Stroudsburg, Pennsylvania' ...
% 'Bowman Dam, California' 'Los Alamos, New Mexico' 'Wind River, Washington' ...

```

```

%      'Lake Spaulding, California' 'Tunkhannock, Pennsylvania' 'Parkdale, Oregon' ...
%      'Sierraville, California' 'Mt. Pocono, Pennsylvania' ...
%      'Cheesman Resvr., Colorado' 'River Falls, Wisconsin' ...
%      'Rimrock Lake, Washington' 'Dannemora, New York' 'Republic, Washington' ...
%      'Wanakena, New York' 'Lake Placid, New York' ...
%      'Wilf1' 'Wilf2' 'Wilf3' 'Wilf4' 'Wilf5' 'Wilf6' 'Wilf7' 'Wilf8' 'Wilf9'];
%... Various options for the calibration calculation
% %... Wolfe 1993 and Wilf 1997 data combined
% x=MAT;
% y=P;
% nfor=nforP;
% %... Wolfe 1993 only
% x=MAT(1:75);
% y=P(1:75);
% nfor=nforP(1:75);
% %... Wilf 1997 only
% x=MAT(76:84);
% y=P(76:84);
% nfor=nforP(76:84);

%=====
%... Select dataset for analysis
%... Wolfe 1993 and Wilf 1997 data combined
x=MAT;
y=P;
nfor=nforP;

%... Overdispersion parameter for the logistic normal variance function
%... phi= 0;
phi= 0.0520;
%... Standard error for P, used to weight the regression
SEy=sqrt((1+phi.*(nfor-1).*y.*(1-y)).*y.*(1-y)./nfor);
N=size(x,1); %... Number of data for regression
%=====
%... Assign weights
;... w=ones(N,1); %... used to give unweighted solution
w=SEy.^(-2);

%... Start regression calculation
Sw=sum(w);
Xbar=sum(w.*x)/Sw;
Ybar=sum(w.*y)/Sw;
Sxx=sum(w.*(x-Xbar).^2);
Syy=sum(w.*(y-Ybar).^2);
Sxy=sum(w.*(x-Xbar).*(y-Ybar));
b=Sxy/Sxx;
a=Ybar-b*Xbar;
SSE=Syy-b^2*Sxx;
%... sigma represents the average residual variance not accounted for by weights
Sigma=sqrt(SSE/(N-2));
ReducedX2=Sigma^2;
SEYbar=Sigma/Sw^0.5; %... Also given by: SEYbar=sqrt(SEa^2- (Xbar*SEb)^2)
R2=(1-SSE/Syy);
SEa=Sigma*sqrt(Sw^-1 + Xbar^2/Sxx);
SEb=Sigma*sqrt(1/Sxx);

disp(sprintf('\n \n'));
disp('=====')
str=sprintf(['PredictMAT.m, Mark Brandon, Yale University, 2006\n' ...
'Estimation of the calibration equation for MAT from P, and\n' ...
'use of that equation to predict MAT from a measurement of P.\n' ...
'The calculations follow the methods in Miller et al. (EPSL, 2006)']);
disp(str)
str=sprintf('Calibration data set includes a total of %g sites.',N);
disp(str)
str=sprintf('Overdispersion parameter is set to phi = %g.\n',phi);
disp(str)

%... Output results
WtFlag= sum(w-ones(N,1));
if WtFlag ==0
    disp('RESULTS: UNWEIGHTED FIT FOR CALIBRATION EQUATION')
    str=sprintf(['N = %g\na = %g\nb = %g\nSE(a) = %g\nSE(b) = %g\nXbar = %g\n' ...
'R^2 = %g\nSigma = %g'], ...
[N a b SEa SEb Xbar R2 Sigma]);
    disp(str)
else
    disp('RESULTS: WEIGHTED FIT FOR CALIBRATION EQUATION')
    str=sprintf(['N = %g\na = %g\nb = %g\nSE(a) = %g\nSE(b) = %g\nXbar = %g\n' ...
'R^2 = %g\nSigma = %g\nReducedX2 = %g'], ...
[N a b SEa SEb Xbar R2 Sigma ReducedX2]);

```

```

disp(str)
end

%=====
%... Calculate confidence limits for MAT predictions at specified
% probability values
Name=strvcat('Chandler(all): Chandler Fm.','Redmond: Redmond Fm.', ...
'Dunvegan: Dunvegan Fm.','Dakota (all): Dakota','Milton: Raritan', ...
'Woodbridge: Raritan','South Amboy: Raritan','Malden Mtn.: Patapsco', ...
'Arthurs Bluff: Woodbine','Denton Co.: Woodbine','Potomac', ...
'Winthrop Fm. ');
P=[0.33 0.52 0.57 0.64 0.78 0.85 0.74 0.77 0.87 0.82 0.6125 0.763]';
%... Set nforP equal to the number of species counted for the measured P value
nforP=[67 23 46 343 27 59 33 26 30 57 40 43]';
%... Enter here specified probability values
%... Probabilities for 95% and 68% confidence intervals
%... probvalues=[0.025 0.1587 0.8413 0.975]';
%... Probabilities for 95% confidence intervals
%... probvalues=[0.025 0.975]';
probvalues=[0.025 0.975]';
X0=MAT;
Y0=P;
nforY=nforP;

disp(' ')
disp('RESULTS: PREDICTIONS FOR MEASURED P VALUES')
str=sprintf(['Right-hand columns show confidence values for MAT for the \n' ...
'probabilities specified in the column headings.']);
disp(str)
str=sprintf('Name \t P\t\t\t\t\t2SE(P)\tMAT(C)');
for j=1:size(probvalues,1),
str=[str sprintf('\t%5.4g',probvalues(j)*100) '%'];
end
disp(str)
%... Calculate values for confidence intervals
for i = 1:size(Y0,1)
SEY=sqrt((1+phi*(nforY(i)-1)*Y0(i)*(1-Y0(i))) * Y0(i)*(1-Y0(i))/nforY(i));
X0=(Y0(i)-a)/b;
str=[Name(i,:) sprintf('%5.3g\t%5.3g\t%5.3g\t%5.3g', ...
[Y0(i) nforY(i) 2*SEY X0])];
for j=1:size(probvalues,1)
%... t statistic to represent confidence interval for the errors
% associated with the regression.
% Note the degrees of freedom are N-2, given that the regression
% requires estimates for two parameters, a and b.
t1=tinv(probvalues(j),N-2);
%... t statistic to represent confidence interval for the errors
% associated with the unknown Y0.
% Note the uncertainties for Y0 are best represented by a gaussian
% (which is equivalent to a t statistic with infinity degrees of freedom).
t2=norminv(probvalues(j));
%... Standard error for P using the logistic normal variance function
SEY0=sqrt((1+phi*(nforY(i)-1)*Y0(i)*(1-Y0(i))) * Y0(i)*(1-Y0(i))/nforY(i));
X0=(Y0(i)-a)/b;
g=(t1*(SEb/b))^2;
SignFlag=(2*(probvalues(j)>0.5)-1);
A=g*(X0-Xbar);
B=(SignFlag/b)*sqrt((t1*SEb*(X0-Xbar))^2+(1-g)*((t1*SEYbar)^2)...
+(t2*SEY0)^2);
DX0conf=(A+B)/(1-g);
str=[str sprintf('\t%5.3g',DX0conf)];
end
disp(str)
end
end

```

OUTPUT FROM ABOVE MATLAB SCRIPT

=====
PredictMAT.m, Mark Brandon, Yale University, 2006 Estimation of the calibration equation for MAT from P, and use of that equation to predict MAT from a measurement of P. The calculations follow the methods in Miller et al. (EPSL, 2006). Calibration data set includes a total of 84 sites. Overdispersion parameter is set to $\phi = 0.052$.

RESULTS: WEIGHTED FIT FOR CALIBRATION EQUATION

N = 84
a = -0.0455705
b = 0.0345339
SE(a) = 0.0225867
SE(b) = 0.00116273
Xbar = 17.9604
R² = 0.914949
Sigma = 0.999949
ReducedX2 = 0.999898

RESULTS: PREDICTIONS FOR MEASURED P VALUES

Right-hand columns show confidence values for MAT for the probabilities specified in the column headings.

Name	P	n	2SE(P)	MAT(C)	2.5%	97.5%
Chandler(all): Chandler Fm.	0.33	67	0.152	10.9	-4.42	4.36
Redmond: Redmond Fm.	0.52	23	0.236	16.4	-6.74	6.73
Dunvegan: Dunvegan Fm.	0.57	46	0.183	17.8	-5.23	5.23
Dakota (all): Dakota	0.64	343	0.117	19.9	-3.36	3.38
Milton: Raritan	0.78	27	0.177	23.9	-5.05	5.1
Woodbridge: Raritan	0.85	59	0.109	25.9	-3.16	3.23
South Amboy: Raritan	0.74	33	0.175	22.7	-5	5.05
Malden Mtn.: Patapsco	0.77	26	0.183	23.6	-5.22	5.27
Arthurs Bluff: Woodbine	0.87	30	0.133	26.5	-3.82	3.89
Denton Co.: Woodbine	0.82	57	0.122	25.1	-3.5	3.56
Potomac	0.613	40	0.188	19.1	-5.35	5.36
Winthrop Fm.	0.763	43	0.153	23.4	-4.38	4.42

>>

CAPTIONS FOR FIGURES IN DATA REPOSITORY

Figure A1. Contribution of uncertainty to the $SE[P]$ accounted for by corrections for overdispersion using the logistic normal variance function. (a) Comparison of the number of species and the percent contribution of uncertainty to the $SE[P]$. This plot shows that the correction for overdispersion accounts for about 15% of the uncertainty in the CLAMP samples (circles), but up to 160% of the uncertainty with samples with $n > 50$ (samples from Wilf (1997) (squares)). This demonstrates the strong dependence of sample size on the uncertainty due to overdispersion. (b) Comparison of P to the percent contribution of uncertainty to $SE[P]$. This plot shows that the overdispersion error is independent on P .

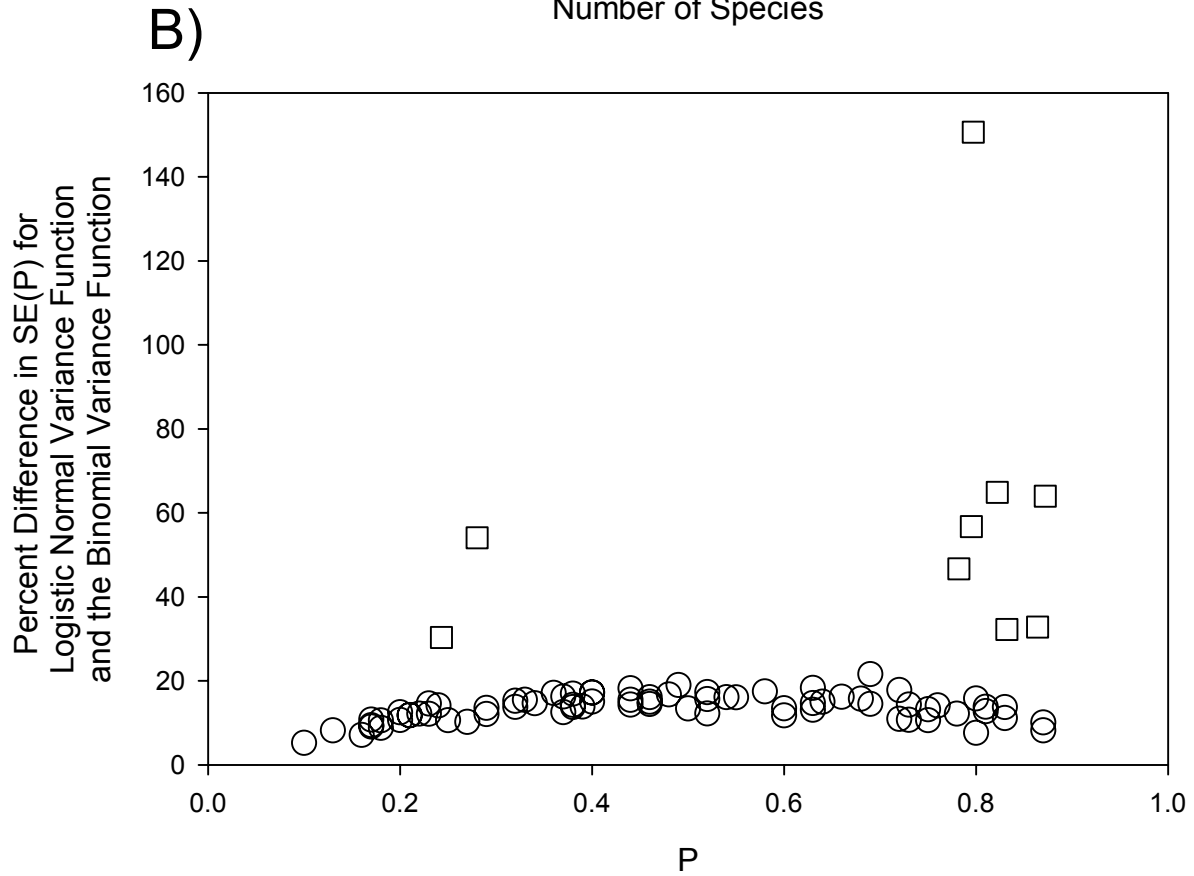
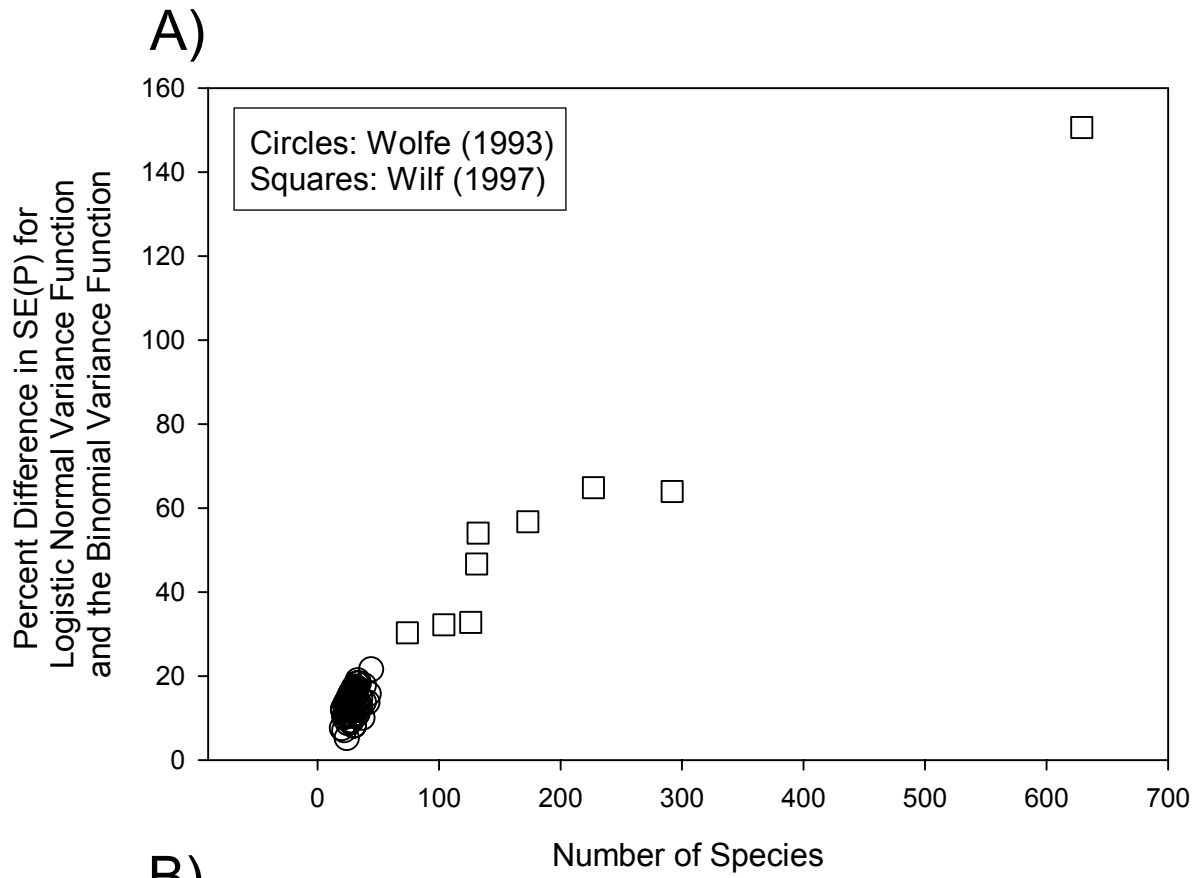
Figure A2. The locations of 1,944 North American weather stations used in the analysis of modern MAT and latitude. Station locations are summarized in the Global Historical Climatology Network (GHCN) temperature archive version 2 dataset (*v2.mean_adj.Z*) (Peterson and Vose 2001).

REFERENCES CITED IN DATA REPOSITORY

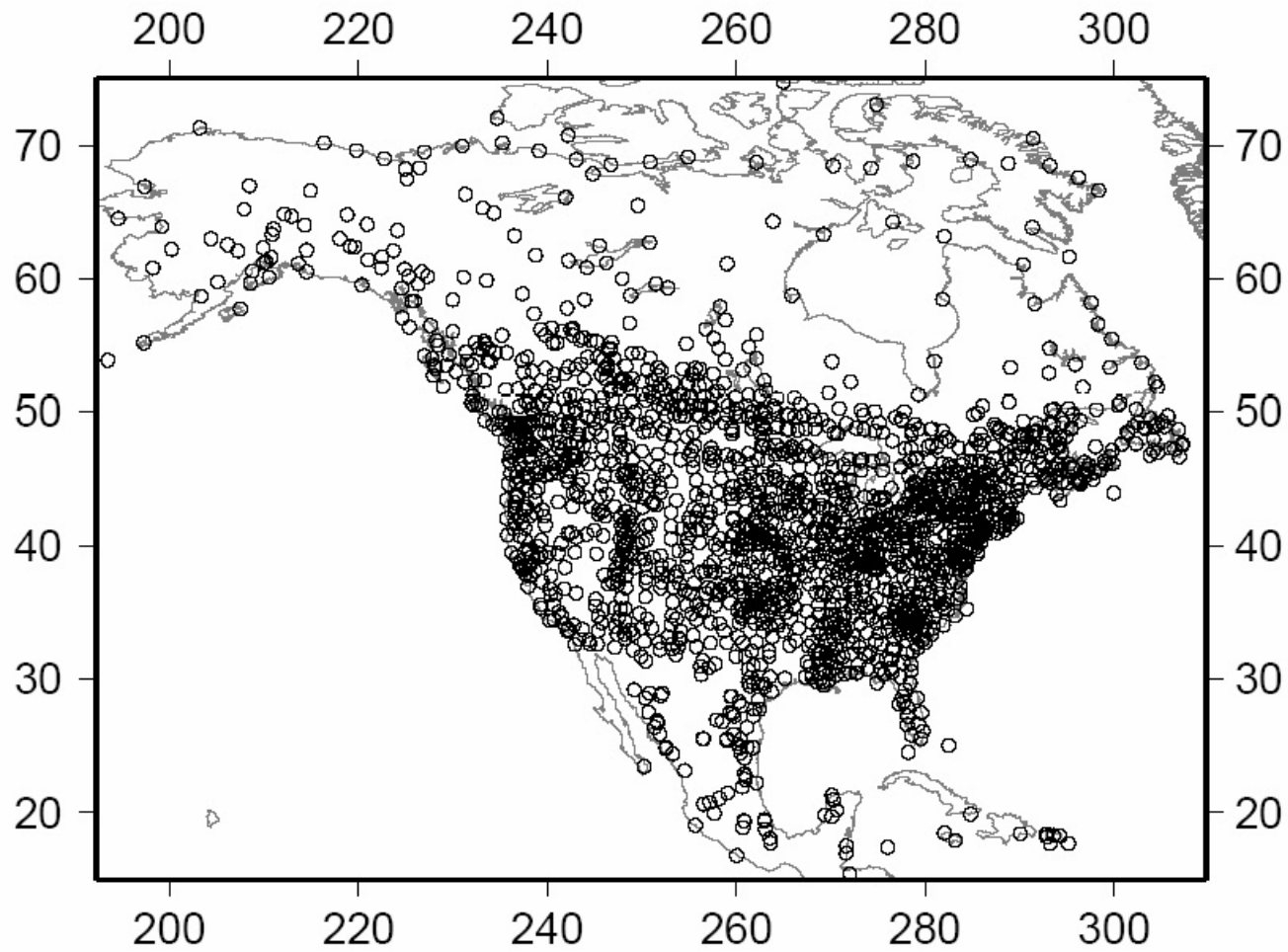
- Chow, S. C. and J. Shao (1990). "On the difference between the classical and inverse methods of calibration." Applied Statistics **39**: 219-228.
- Draper, N. R. and H. Smith (1998). Applied Regression Analysis, Third Edition. Series in Probability and Statistics. Wiley and Son, Inc., 706 p,
- Osborne, C. (1991). "Statistical calibration: A review." International Statistical Review **59**: 309-336.
- Peterson, T. C. and R. S. Vose (2001). An overview of the Global Historical Climatology Network temperature database,
<http://lwf.ncdc.noaa.gov/oa/climate/research/ghcn/ghcnoverview.html> Data archive is at: <http://dss.ucar.edu/datasets/ds564.0/data/ver2/ghcnftp.html>.
- Wilf, P. (1997). "When are leaves good thermometers? A new case for leaf margin analysis." Paleobiology **23**: 373-390.
- Wolfe, J. A. (1993). "A method of obtaining climatic parameters from leaf assemblages." U.S.G.S. Professional Paper **1106**: 1-37.

Miller et al. Figure A1

Comparison of SE(P) for the Logistic Normal Variance Function Relative to the Binomial Variance Function



North American GHCN Station Locations



Miller et al., Figure A2